



## Seismogenic permeability, $k_s$

Pradeep Talwani,<sup>1</sup> Linyue Chen,<sup>1,2</sup> and Kalpna Gahalaut<sup>3</sup>

Received 29 July 2006; revised 6 December 2006; accepted 14 March 2007; published 10 July 2007.

[1] The temporal and spatial pattern of seismicity associated with reservoir water level fluctuations, injection of high-pressure fluids in deep boreholes, and seasonal groundwater recharge provide a unique setting to study the hydrological properties of the seismogenic fractures. Pore pressure diffusion is primarily responsible for the build up of fluid pressures and the onset of seismicity. The hydrologic property controlling pore pressure diffusion is hydraulic diffusivity  $c$ , which is directly related to intrinsic permeability  $k$ . By analyzing more than 90 case histories of induced seismicity, we determined the hydraulic diffusivity value of fractures associated with seismicity to lie between 0.1 and 10 m<sup>2</sup>/s. This range of values of  $c$  corresponds to a range of intrinsic permeability values between  $5 \times 10^{-16}$  and  $5 \times 10^{-14}$  m<sup>2</sup>. We call this range the seismogenic permeability  $k_s$ . Fractures with  $k_s$  were found to be associated with Darcian flow. Fractures with permeability less than  $k_s$  were aseismic, as the pore pressure increase was negligible. In fractures with permeability larger than  $k_s$ , aseismic non-Darcian flow was observed. Seismicity was uniquely associated with fractures with seismogenic permeability. Thus seismogenic permeability is an intrinsic property of fractures where pore pressure diffusion is associated with seismicity.

**Citation:** Talwani, P., L. Chen, and K. Gahalaut (2007), Seismogenic permeability,  $k_s$ , *J. Geophys. Res.*, 112, B07309, doi:10.1029/2006JB004665.

### 1. Introduction

[2] Temporal and spatial patterns of induced seismicity following the impoundment of a reservoir, or the injection of fluids in a well, or seasonal groundwater recharge provide evidence for the predominant role of fluid pressure diffusion in their generation. The rate of epicentral growth, the time lag between reservoir impoundment, or fluid injection in a well, and the onset of seismicity were the elements used by *Talwani and Acree* [1984] to estimate the hydraulic diffusivity  $c$ , and therefrom, the intrinsic permeability  $k$  of the fractured rocks associated with seismicity. For most of the  $\sim 50$  cases of reservoir- and injection-induced seismicity (RIS and IIS), they found the intrinsic permeability to range between  $10^{-16}$  and  $10^{-14}$  m<sup>2</sup>. Shapiro and coworkers applied the same concept to estimate the permeability from the hypocentral growth of fluid-injection-induced seismicity at KTB (Kontinentale Tiefbohrung) site in Germany [*Shapiro et al.*, 1997] and at hot dry rock (HDR) sites at Fenton Hill, USA and Soultz, France [*Shapiro et al.*, 2003]. For these cases, where seismicity followed high-pressure fluid injections, they found  $k$  to be  $\sim 10^{-17}$  to  $10^{-16}$  m<sup>2</sup>. However, for the aftershock pattern of the Antofagasta, Chile earthquake of 1995, they estimated  $k$  to be  $6 \times 10^{-14}$  m<sup>2</sup>.

[3] *Saxena et al.* [1988] used Biot's consolidation theory in developing a model for reservoir-induced seismicity by simulating fractures under a reservoir as fluid-filled elastic material. They considered the overburden pressure due to reservoir impoundment to be the maximum stress responsible for destabilizing the fractures according to Mohr-Coulomb fracture failure criterion. They considered such failure as an induced event and presented their result in terms of number of such events. They suggested that the frequency of such events was dependent on the "time taken" for the pore pressure buildup and was thus dependent on the reservoir-filling history and the coefficient of hydraulic conductivity,  $K = kg\rho/\mu$ , where  $k$  is permeability,  $g$  is the acceleration due to Earth's gravity, and  $\rho$  and  $\mu$  are the density and dynamic viscosity of water, respectively. They found that the frequency of induced seismicity was highest when  $K$  ranged between  $\sim 10^{-9}$  and  $10^{-7}$  ms<sup>-1</sup>. Taking  $\mu = 10^{-3}$  Pa s and  $\rho = 10^3$  kg m<sup>-3</sup>, the range of  $K$ ,  $10^{-9}$  to  $10^{-7}$  ms<sup>-1</sup>, corresponds to an intrinsic permeability,  $k$ , range of  $10^{-16}$  to  $10^{-14}$  m<sup>2</sup>. In these examples of RIS, the exact nature of the subsurface fractures connecting the reservoir to the hypocentral locations is largely unknown.

[4] In the last two decades, fluid-injection-induced seismicity (IIS) has been studied at various locations. Targeted studies were carried out in crystalline rocks in a large granite block in France [*Cornet and Yin*, 1995] at the KTB site in Germany [*Zoback and Harjes*, 1997] and in the Philippine and Nojima Fault Zones [*Prioul et al.*, 2000; *Tadokoro et al.*, 2000]. Other targeted studies of IIS were carried out at locations of hot dry rock projects, for example, at Soultz, France [*Evans et al.*, 2005] and at the Hijiori hot dry rock site in Japan [*Sasaki*, 1998; *Tezuka and*

<sup>1</sup>Department of Geological Sciences, University of South Carolina, Columbia, South Carolina, USA.

<sup>2</sup>Harrison, New Jersey, USA.

<sup>3</sup>National Geophysical Research Institute, Hyderabad, India.

Niitsuma, 2000]. At these locations the availability of detailed fluid pressure histories at the surface and at hypocentral locations have helped to assess the conclusions based mainly on RIS and aftershock data on a characteristic range of intrinsic permeability of fractures associated with fluid-induced seismicity.

[5] More recently, it has been possible to estimate hydraulic diffusivity in regions where an association was established between intense rainfall or groundwater recharge due to snowmelt and seismicity [Hainzl *et al.*, 2006; Saar and Manga, 2003].

[6] In order to see if there is a characteristic value of permeability of fractures wherein the seismicity is associated with fluid pressure diffusion, we greatly expanded our database. Before presenting the results of this exercise, we present first some background information related to pore pressures in fluid-filled fractures and the genesis of reservoir-induced seismicity. Then we present our results and discuss their implications in light of the more recent and detailed IIS data.

## 2. Background

### 2.1. Pore Pressure Flow Occurs Through Discrete Fractures

[7] From a study of exhumed faults in the upper brittle regions of the crust, Sibson [2001] noted that major trans-crustal fault zones are predominantly tabular. Cornet and Yin [1995] monitored induced seismicity and fluid flow associated with large-scale forced water circulation in  $\sim 15 \times 10^6 \text{ m}^3$  volume of granite at Le Mayet de Montagne in central France. They found that >80% of the flow was contained in three or four main preexisting fractures. A similar observation was made by Evans *et al.* [2005] in a hot dry rock experiment at Soultz-sous-Forêts in the Rhine Graben near Strasbourg, France. There,  $\sim 20,000 \text{ m}^3$  of water was injected into the granite between 2.8- and 3.4-km depth in September 1993. These authors found that during injection,  $\sim 95\%$  of the flow into the rock mass was confined to just 10 major, naturally occurring permeable fractures. In an experimental determination of in situ hydraulic properties of a shear zone in northwest South Carolina, Talwani *et al.* [1999] compared water levels in a reservoir with those in an observation well, 250 m away, connected to the reservoir by a 1-m-wide shear zone. The shear zone was one of six such zones embedded in a crystalline rock matrix, encountered at the bottom of the reservoir. Experimental results and direct observations in the underground tunnels and in the powerhouse area below the reservoir indicated that these saturated shear zones were the only conduits for fluid and fluid-pore pressure flow away from the reservoir. In this paper we will use the more common terminology, pore pressure, for fluid-pore pressure.

[8] These three examples in diverse locations illustrate an important observation. In fractured crystalline rocks, when elevated pore pressures are applied at the bottom of a reservoir due to lake impoundment, or at an injection site in a well, the hydraulic response is confined to relatively few saturated, planar fractures, while the surrounding rocks respond elastically. These observations further illustrate that “the concept of permeability of an equivalent continuum” fails for these crystalline rocks [Cornet and Yin, 1995].

Evans *et al.* [2005] used “equivalent porous medium” permeability to reflect this difference with ordinary sedimentary rocks.

### 2.2. Critically Stressed Permeable, Saturated Fractures

[9] In situ stress data and knowledge of the orientation of permeable saturated fractures obtained from borehole data were used by Barton *et al.* [1995] to compute the maximum shear and normal stress components on the fractures. For different stress regimes, for an assumed coefficient of friction between 0.6 and 1.0, these fractures were “critically stressed,” i.e., on the verge of failure. Observations of Barton *et al.* [1995] have been confirmed in subsequent studies. For example, Evans *et al.* [2005] studied the stress field and fractures at the hot dry rock site at Soultz, France. In the 3.6-km deep hole,  $\sim 500$  natural fractures were imaged using a borehole televiewer. Of these, 18 were naturally permeable fractures, and all of them were found to be “critically stressed.” By analyzing the permeable fractures encountered in the KTB scientific main hole, Ito and Zoback [2000] showed that the critically stressed faults were also the most permeable.

[10] In summary, the results of Barton *et al.* [1995], and subsequent studies, [e.g., Townend and Zoback, 2000], show that saturated permeable fractures tend to be “critically stressed” and are on the verge of failure. In cases of RIS and IIS, fluid pressure increases can lead to failure, which we describe next.

### 2.3. Coulomb Failure Criterion

[11] The frictional strength  $S$  of a fault is governed by the Coulomb failure criterion [Jaeger and Cook, 1969],

$$S = S_0 + \mu(\sigma_n - p) - \tau \quad (1)$$

where  $S_0$  is cohesion,  $\mu$  is the coefficient of friction,  $\sigma_n$  and  $\tau$  are the normal and the shear stresses, respectively, and  $p$  is the pore pressure. Compression is taken as positive. Impoundment of a reservoir can induce seismicity by lowering the strength  $S$  (or equivalently, by increasing the Coulomb failure stress) by mechanical or chemical effects of water on  $S_0$ ,  $\mu$ ,  $\sigma_n$ ,  $\tau$ , and  $p$ . This can be accomplished by an increase in pore pressure,  $\Delta p$ .  $\Delta p$  due to reservoir impoundment or lake level fluctuations is usually much smaller than  $\sigma_n$ ; however, in the case of IIS, it can exceed  $\sigma_3$ , the least principal stress. Shear slip can occur when the additional pore pressure is a fraction of  $\sigma_3$ . The onset of shear slip along the fractures depends on their orientation with respect to  $\sigma_3$  (Figure 1) [Tezuka and Niitsuma, 2000]. Full fracture opening occurs only when pore pressures exceed  $\sigma_3$ . In that case, they dilate, increasing the fracture permeability and promoting fluid flow. The opening of fractures due to tensile failure is referred to as fracture-normal-dilation [Evans *et al.*, 2005], or “jacking,” and is one of the objectives in hot dry rock experiments.

### 2.4. Effect of Rate of Change of Pore Pressure

[12] Detailed case histories at locations of IIS provide another parameter that had earlier been suggested to affect the seismicity pattern. Nur and Booker [1972] showed that, when aftershocks could be attributed to pore pressure changes, their frequency was proportional to the rate of pore pressure increase. Bosl and Nur [2002] used this

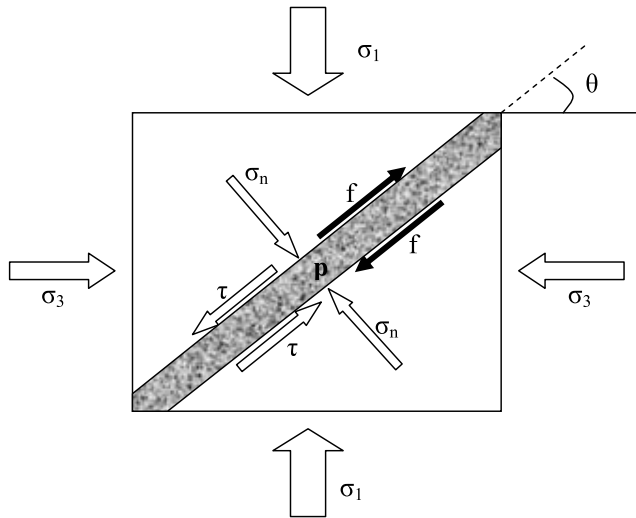


**Figure 1.** A fluid-filled fracture with pore fluid pressure  $p$  subjected to a two-dimensional stress field.  $\sigma_n$ ,  $\tau$ , and  $f$  are the normal, shear, and frictional stresses, respectively (modified from the work of *Tezuka and Niitsuma* [2000]).

concept to explain the 1992 Landers earthquake sequence. In the case of RIS, water level changes are directly related to pore pressure changes below the reservoir (next section). The results of modeling [*Saxena et al.*, 1988] and empirical evidence at *Koyna Reservoir* [*Gupta*, 1983] also relate an increase in seismicity to an increase in the rate of filling, i.e., to the rate of increase in pore pressure. Next, we present some background on the mechanism of reservoir-induced seismicity.

**2.5. Mechanism of RIS**

[13] Induced seismicity is caused by shear failure along a preexisting fault plane in accordance with the Coulomb failure criterion (1). The change in strength, due to impoundment of a reservoir and changes in lake levels can induce seismicity on two timescales. First is an immediate, undrained, elastic response to loading, and second is a delayed response due to diffusion of pore pressure (a detailed discussion is presented by *Chen and Talwani* [2001]). Here we briefly describe the two effects. The instantaneous undrained effect manifests itself in two ways: first, the elastic response to the reservoir load, and second, an instantaneous pore pressure change in the vicinity of the reservoir due to an undrained response [*Skempton*, 1954].

[14] This undrained response, also referred to as the pore pressure increase due to compression, at any point P at a distance  $r$  from the bottom of the reservoir (Figure 2), is

$$\Delta p_u(r) = B\Delta\sigma_{av} \tag{2}$$

where,  $\Delta\sigma_{av}$  is the change in the average normal stress at P, and  $B$  is the Skempton’s coefficient.  $B$  is the ratio of the incremental change in pore pressure and the average normal stress and is  $\sim 0.7$  for crystalline rocks [*Talwani et al.*, 1999];  $\Delta p_u(r)$  varies from  $\sim 0.7$  times the average compressive stress increase at the bottom of the reservoir, A, ( $r = 0$ ), to zero at a distance  $r_0$ . For  $r > r_0$ ,  $\Delta p_u(r) = 0$ , (Figure 2).

[15] Both this increase in pore pressure due to an undrained response to loading and that at the bottom of the reservoir because of impoundment diffuse away along suitably located, saturated fractures, thus causing a delayed increase in  $\Delta p$  and failure.

[16] The delayed response can also be divided into two parts. First is by an increase in pore pressure by diffusion from A to  $Q_1$  and  $Q_2$  along discrete fractures, and second, a decrease in pore pressure by relaxation, i.e., the diffusion of  $\Delta p_u(r)$  along a fracture from P to  $Q_3$ . If P ( $r \leq r_0$ ) is also connected to A by a fracture, we have a coupled effect, an increase in pore pressure by diffusion from A to P, and a pore pressure decrease by diffusion of  $\Delta p_u$  away from P. When  $r > r_0$ , we have only a delayed pore pressure increase at  $Q_2$ . The latter is the most common cause of the observed delay between the filling of reservoirs and the pursuant seismicity.

[17] We next use the ideas presented above to formulate the poroelastic response of the substratum to reservoir impoundment.

**3. Poroelastic Response**

[18] To study the poroelastic response of the subsurface to reservoir impoundment and lake level fluctuations, we assume that we are dealing with fluid-filled fractures and not with a uniform half-space. We further assume that the fracture permeability is much larger than that of the host rocks so that all fluid pressures are confined to the fractures. Following the work of *Barton et al.* [1995] and *Townend and Zoback* [2000], we consider all saturated fractures to be critically stressed so that small changes in fluid pressures

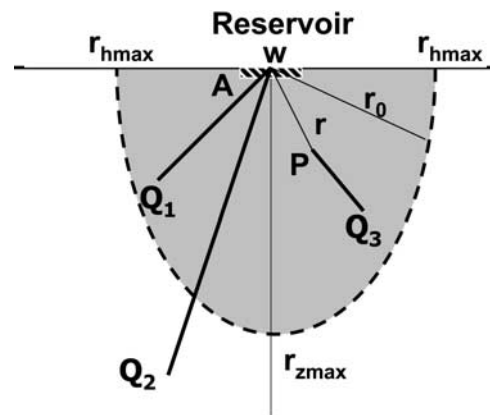


**Figure 2.** The instantaneous affect of loading a reservoir of width  $w$  occurs within the shaded area, at a distance  $r_0$  from the bottom of the reservoir, A. The distance  $r_0$  varies from  $r_{zmax}$  below the reservoir to  $r_{hmax}$  near the surface. These distances are 6 to 7 and 3 to 4 times the width of the reservoir,  $w$ , respectively. The undrained, instantaneous pore pressure increases at any point A or P is  $B$  times the average stress increase at that location, where  $B$  is the Skempton’s coefficient. The delayed pore pressure increases at  $Q_1$ ,  $Q_2$ , and  $Q_3$  occur because of the pore pressure diffusion along discrete fractures (solid lines) connecting them to sources of instantaneous elevated pressures at A and P, respectively. If P is connected to A by a discrete fracture there will be a coupled effect at P (see text for details).

can trigger seismicity. With these assumptions pore pressure diffusion is confined to critically stressed, permeable, pre-existing fractures, such that small changes in pore pressures leads to seismicity according to the Coulomb failure criterion. We also assume that these fractures can be mathematically represented by one- and two-dimensional models. We make the same assumptions when dealing with seismicity related to fluid injections in a borehole, seasonal or volcanic activity. Following the work of *Nur and Booker* [1972] we assume that the rate of change of pore pressure is related to the number of earthquakes. In view of the observed delay between filling and seismicity in almost all known cases of induced seismicity, we conclude that the seismicity is primarily associated with the diffusion of pore pressure [Talwani, 1997; Chen and Talwani, 2001]. This pore pressure diffusion causes a time lag between the onset of filling and the pursuant seismicity. The efficiency of pore pressure diffusion depends on the hydraulic properties of the fractures and is discussed in a later section.

[19] *Roeloffs* [1988] calculated the coupled poroelastic response at point  $P(r)$  (Figure 2) due to reservoir impoundment. For one-dimensional pore pressure diffusion along narrow fractures with hydraulic diffusivity  $c$  (assuming no loss of fluid pressure to outside the fracture), she found that the solution to a one-dimensional fully coupled pore pressure diffusion equation gives the pore pressure at a distance  $r$ , at a time  $t$ , to be,

$$p(r, t) = \alpha p_0 \operatorname{erf} \left[ \frac{r}{(4ct)^{1/2}} \right] + p_0 \operatorname{erfc} \left[ \frac{r}{(4ct)^{1/2}} \right] \quad (3)$$

where  $p(0, t) = p_0$ , and  $p_0 = 0$  for  $t < 0$  and  $p_0 = 1$  for  $t > 0$ , and  $\alpha$  is an elastic constant related to  $B$  and the undrained Poisson's ratio.

[20] In equation (3), the first term represents the undrained response of the fracture at time  $t = 0$  and its poroelastic relaxation at  $t > 0$ . The second term represents the pore pressure induced by diffusion at a distance  $r$  due to an applied load at the surface.

[21] We note from equation (3) that, on impoundment at  $t = 0$ ,  $p(r, t) = \alpha p_0$  (the undrained effect due to compression) and, at  $t = \infty$ ,  $p(r, t) = p_0$  (there is only the drained effect due to diffusion).

[22] The pore pressure changes at hypocentral depths associated with the impoundment of a reservoir depend on its filling history. For a time-varying reservoir load, these can be obtained from equation (3) by the principle of superposition. We get

$$P_i(r, t) = \sum_{i=1}^n \alpha \delta p_i \operatorname{erf} \left[ \frac{r}{(4c\delta t_i)^{1/2}} \right] + \sum_{i=1}^n \delta p_i \operatorname{erfc} \left[ \frac{r}{(4c\delta t_i)^{1/2}} \right] \quad (4)$$

where  $n$  is the number of time increments,  $\delta t_i$ , between the start of impoundment and the time  $t$ , and  $\Delta p_i$  are water load changes in each corresponding time increment.

### 3.1. Two Examples

[23] There is a twofold response of a fracture when the pore pressure is increased at one end, the diffusion of pore pressure (undrained response) and fluid flow (drained response). The relative values of these effects depend on the hydraulic diffusivity of the fracture and determine if the fracture is seismogenic or not. The seismogenic behavior of

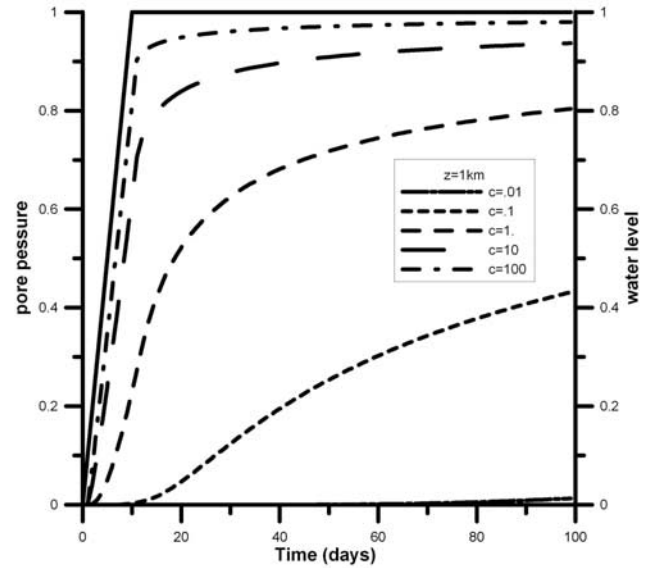


**Figure 3.** The filling curve at reservoir where the water level is maintained after impoundment (solid line). The dashed curves show the corresponding increase in the pore pressure diffusion at a depth of (a) 1 km and (b) 3 km for various diffusivity values (in square meters per second), and (c and d) their rate of change ( $dp/dt$ ) at those depths. The pore pressures are normalized with respect to the pore pressures corresponding to the lake levels. After the initial filling, an increase in the  $dp/dt$  (shaded area) occurs at 1- and 3-km depths corresponding to  $c = 0.1$  and  $1 \text{ m}^2/\text{s}$ , respectively (Figures 3c and 3d).

the fracture depends on the rate of increase of pore pressure,  $dp/dt$ , and the rate of the fluid flow. An increase in  $dp/dt$  leads to seismicity, whereas an increase in fluid flow rates causes a decrease in  $dp/dt$  and an absence of seismicity.

[24] Thus it is the timescales of pore pressure diffusion and the drained response (fluid flow) that determine the response of the fracture. The initial increase in pore pressure, in turn, depends on the rate of filling of the reservoir or the application of injection pressures. We illustrate the roles of these factors with an examination of two filling histories commonly observed in RIS. The conclusions derived from these two examples can be applied to other situations where pore pressure diffusion through saturated fractures is associated with seismicity.

[25] We consider two cases, one in which a reservoir is filled and then the water level is maintained thereafter; this is the case for pumped storage facilities. In the second case, we consider cyclic filling and emptying of a reservoir (for example, at Koyna in India). The curves of the total effect [equation (4)] are similar to those due to diffusion only, the second term on the right side of equation (4). For clarity, in Figures 3 and 4, we consider the buildup of pore pressure due to diffusion, the second term on the right side in equation (4), and its rate of change with time at depths of 1 and 3 km below the reservoir. The time rate of change of pore pressure is used as a proxy for the number of earthquakes (section 2.4). The pore pressures are calculated for a range of values of hydraulic diffusivity  $c$ .

[26] In the first case (Figures 3a, 3b, 3c, and 3d), the reservoir is filled in 10 days (solid line) and then the water

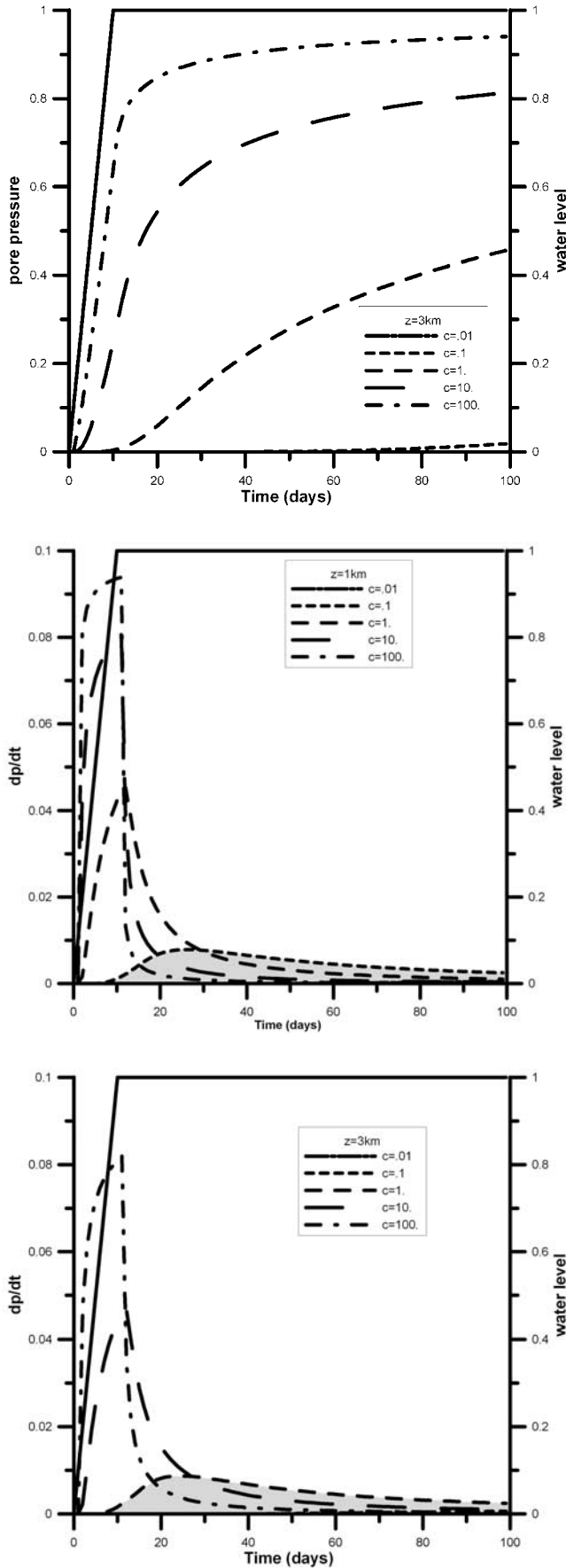


Figure 3. (continued)

level is maintained thereafter. The corresponding increase in pore pressure at any depth, normalized with respect to the lake level, depends on the hydraulic diffusivity  $c$ . At a depth of 1 km, the rise in pore pressure is faster for higher diffusivity values, and for very small values of  $c$  ( $0.01 \text{ m}^2/\text{s}$ ), there is no appreciable increase in pore pressure (Figure 3a). At 3-km depth, the pore pressure increase is similar but muted and appreciable only for values of  $c \geq 1 \text{ m}^2/\text{s}$ .

[27] For large diffusivity values (10 and  $100 \text{ m}^2/\text{s}$ ), the curves showing  $dp/dt$  follow the filling curve and, on completion of filling, decay rapidly (Figures 3c and 3d). At 1-km depth, only the curve corresponding to  $c = 0.1 \text{ m}^2/\text{s}$  shows an increase in  $dp/dt$ , 10 to 20 days after the reservoir

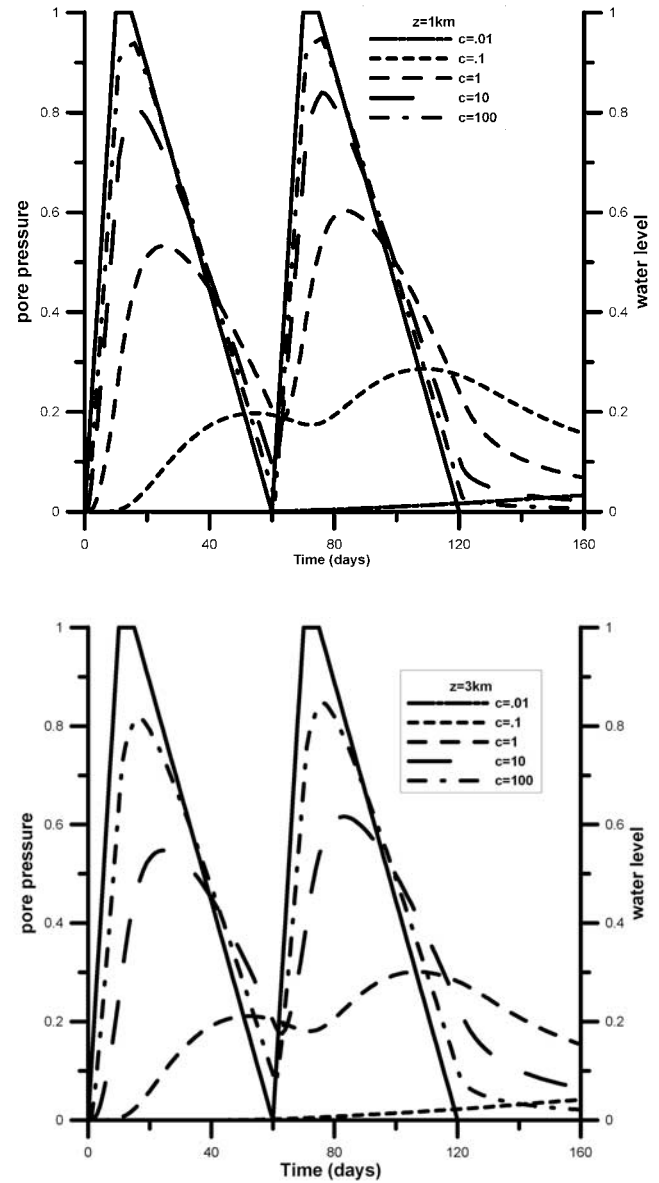


Figure 4. (a and b) Two cycles of filling (solid line) and the corresponding normalized changes in pore pressures due to diffusion at depths of 1 and 3 km for various diffusivity values (in  $\text{m}^2/\text{s}$ ). The rate of change of pore pressure ( $dp/dt$ ) at these depths is shown in Figures 4c and 4d. (c and d) An increase in  $dp/dt$  after the filling (shaded areas) occurs at 1- and 3-km depths for  $c = 0.1$  and  $1 \text{ m}^2/\text{s}$ , respectively.

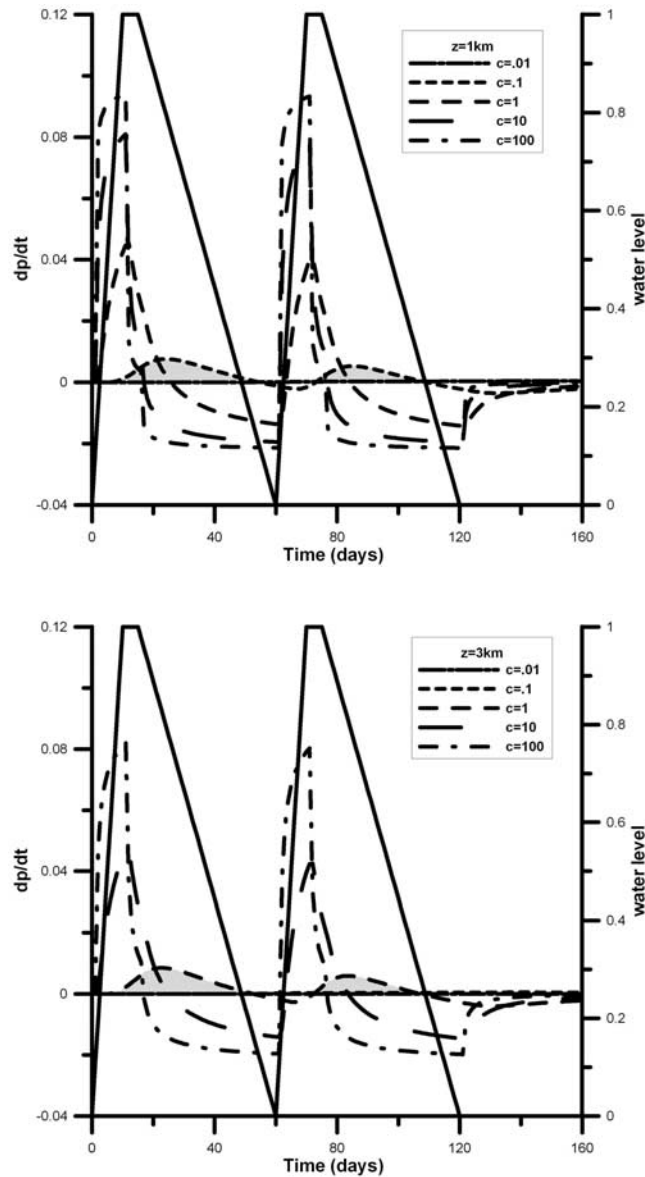


Figure 4. (continued)

is full (At Monticello Reservoir, the peak seismicity was observed about 3 weeks after filling and was concentrated in the top  $\sim 1$  km [Talwani and Acree, 1984]). Figure 3d shows that, at 3-km depth, a delayed increase in  $dp/dt$  occurs when  $c = 1 \text{ m}^2/\text{s}$ . For smaller values of  $c$ , the increase in  $dp/dt$  is negligible. We note that delayed increases in  $dp/dt$  are only observed with  $c = 0.1 \text{ m}^2/\text{s}$  at 1-km depth and with  $c = 1 \text{ m}^2/\text{s}$  at 3-km depth; that is, for both very large and very small values of  $c$ , we do not observe a delayed increase in  $dp/dt$ . Following the work of Nur and Booker [1972] if the frequency of seismicity is proportional to the rate of pore pressure increase, we conclude that the seismicity associated with reservoir impoundment is inhibited by both very large values of  $c$  ( $>10 \text{ m}^2/\text{s}$ ) and by very small values of  $c$  ( $\sim 0.01 \text{ m}^2/\text{s}$ ).

[28] Figures 4a, 4b, 4c, and 4d show similar results for two cycles of reservoir impoundment and emptying. The reservoir is filled in 10 days, maintained for 5 days, and then emptied over the following 45 days. The figures show

the pore pressures (normalized with respect to the lake level) at depths of 1 and 3 km below the reservoir and the corresponding values of  $dp/dt$ . Again, for very large values of  $c$ , the pore pressure increase and decrease follows the lake levels and is negligible for  $c = 0.01 \text{ m}^2/\text{s}$  (Figures 4a and 4b), and the delayed increases in  $dp/dt$  are only observed at a depth of 1 km for  $c = 0.1 \text{ m}^2/\text{s}$  and at 3-km depth for  $c = 1 \text{ m}^2/\text{s}$ . There is a delayed decrease in  $dp/dt$  for larger values of  $c$ , implying a cessation of seismicity.

[29] Figures 5a and 5b compare the results of pore pressure  $p$  and  $dp/dt$  changes at a depth of 3 km, associated

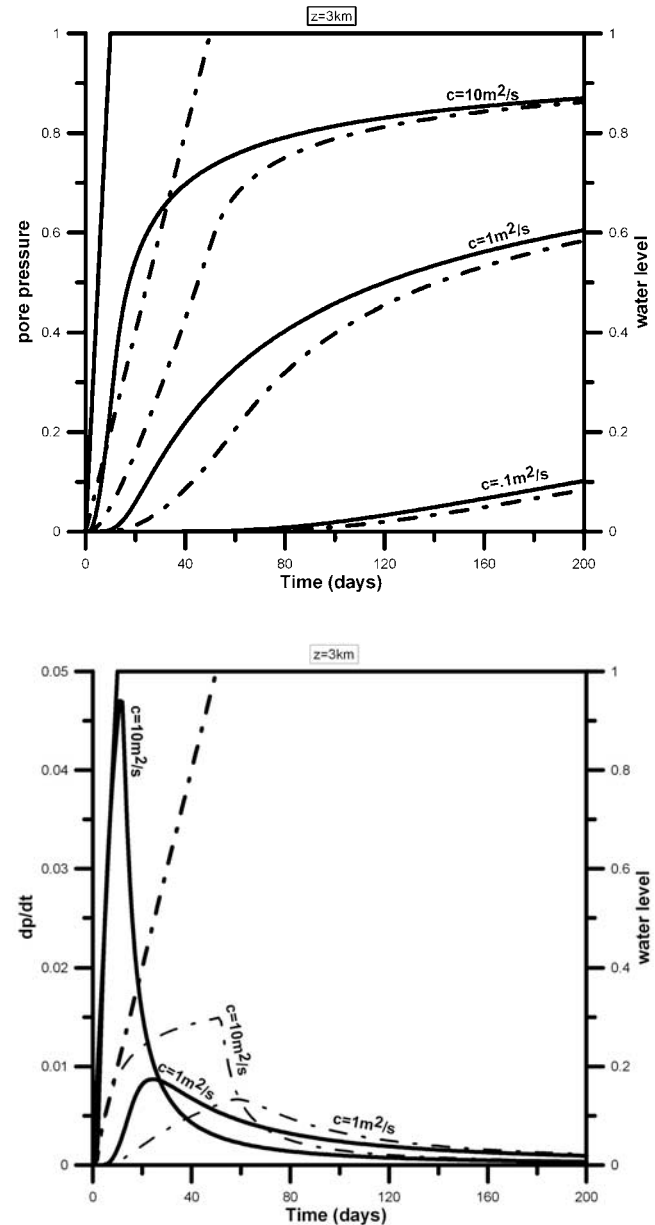
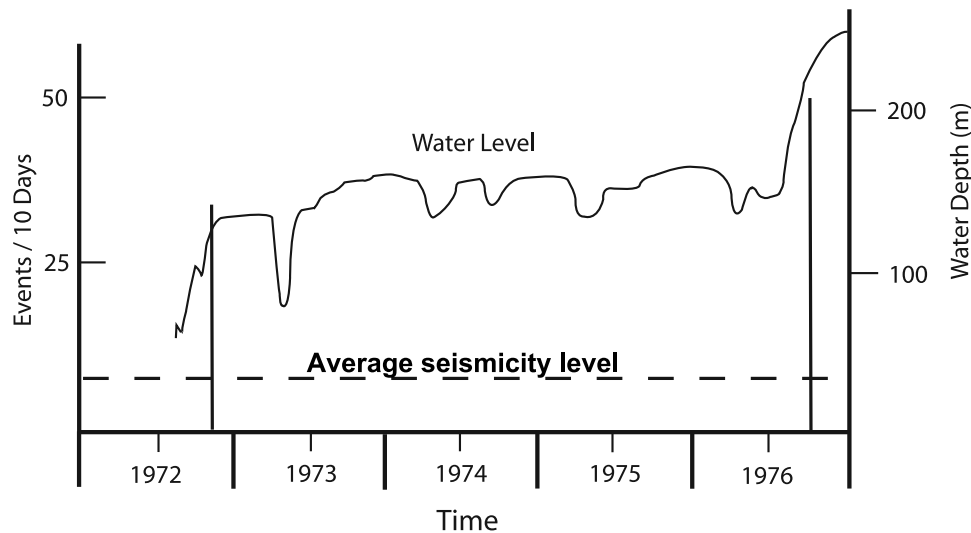


Figure 5. (a) Comparing normalized pore pressures at a depth of 3 km for two different values of  $c$  (in square meters per second) for two filling curves, (b) and the corresponding changes in  $dp/dt$  for  $c = 10.0$  and  $1.0 \text{ m}^2/\text{s}$ . The solid and dashed lines are for reservoir impoundment in 10 and 50 days, respectively, after which the water level is maintained.



**Figure 6.** The times of increased seismicity (vertical lines) that followed increases in lake levels in July 1972 and June 1976 at Nurek reservoir. The time lags between times of lake level increases and seismicity onset were used to calculate hydraulic diffusivity (modified from the work of *Simpson and Negmatullaev* [1981]).

with the filling of a reservoir in 10 and 50 days. In both cases the pore pressure increase follows the filling curves, being slower for smaller diffusivities (Figure 5a). However, there is a significant decrease in the delayed increase in  $dp/dt$  for the slower filling curve when  $c = 10 \text{ m}^2/\text{s}$ . This decrease is less when  $c = 1 \text{ m}^2/\text{s}$ .

[30] The lake level curves presented in Figures 3, 4, and 5 are representative of the filling curves of most reservoirs associated with seismicity. They suggest that the delayed increase in pore pressure associated with filling (or an increase in lake level) occurs for a narrow range of hydraulic diffusivity values (shaded areas in Figures 3c and 3d and 4c and 4d) and is not observed for very large or very small values of  $c$ . There is a negligible increase in  $dp/dt$  for small values of  $c$ . For large values of  $c$ , there is an increase in fluid flow and an absence of delayed increases in  $dp/dt$ . We also note that, when the reservoir is filled slowly, it allows for a greater amount of fluid flow, and correspondingly, a smaller increase in  $dp/dt$ , compared to the case when the reservoir was filled rapidly.

[31] We illustrate the validity of this conclusion with examples of seismicity associated with impoundment of reservoirs, injection of fluids, migration of aftershocks, and seasonal groundwater recharge. In each case we use the temporal pattern of seismicity to estimate  $c$ , and therefrom, the intrinsic permeability  $k$  of fractures associated with pore pressure diffusion.

#### 4. Estimation of Hydraulic Diffusivity, $c$

[32] Reservoir-induced seismicity is primarily associated with pore pressure diffusion in discrete, saturated, critically stressed fractures. The diffusing pore pressure front raises the pore pressure in hypocentral regions and triggers seismicity in accordance with the Coulomb failure criterion (1). The pore pressure front is limited to discrete, planar fractures

connecting the reservoir and the hypocentral region, so that we can assume one-dimensional pore pressure diffusion between the two and use the spatial and temporal pattern of induced seismicity to estimate the hydraulic diffusivity  $c$  of the seismogenic fractures [see, e.g., *Talwani and Acree*, 1984].

[33] *Scholz et al.* [1973] and *Whitcomb et al.* [1973], among others, noted that the time lag,  $\Delta t$ , associated with the diffusion of fluid (pressure) over a distance  $r$  was proportional to  $r^2/c$ . They assumed  $\Delta t = r^2/c$ , a relationship used by *Talwani and Acree* [1984] to estimate  $c$  from the temporal pattern of induced seismicity.

[34] However, *Wang* [2000, p. 123] has shown that the time  $t$  taken for surface pressure to propagate diffusively to a depth  $z$  is given by  $t = z^2/4c$ . *Kessels and Kück* [1995] showed that, for fluid injection in a borehole, considered as a linear line source, the time  $t$  for the maximum pressure to diffuse a distance  $r$  from the borehole along a fracture is also given by  $t = r^2/4c$ .

[35] Therefore, in cases of induced seismicity, if we know the time lag  $\Delta t$  between the impoundment of a reservoir, or the start of fluid injection in a well, and the onset of seismicity at a distance  $r$ , we can estimate the hydraulic diffusivity  $c$  of the connecting fractures from

$$c = r^2/4\Delta t \quad (5)$$

[36] In some cases, where the fractures are closer to horizontal, the impoundment of a reservoir, or the injection of fluids in a well, results in growing epicentral areas; the temporal growth of the epicentral area is related to the hydraulic diffusivity, and the slope of the epicentral area versus time curve can be used to estimate  $c$  [*Talwani and Acree*, 1984]. In other cases the hydraulic diffusivity can be estimated from the migration rate of the aftershocks. In rare cases, estimates of fracture transmissivity  $T$  and storativity  $S$  obtained by pumping tests for fractures cut by an injection

**Table 1.** Estimates of Hydraulic Diffusivity,  $c$  ( $m^2/s$ )

Method	<0.1	0.1–1.0	1.0–10.0	>10.0
Time Lag for RIS	1	19	16	
Time Lag for IIS		2	8	
Area Growth RIS		5	4	1
Area Growth IIS	1	6	2	
Precursors		3	7	
Time Lag for Seasonal Seismicity Measurement		4	6	1
Total	2	40	44	2

well can be used to calculate  $c$  ( $c = T/S$ ) [e.g., Hsieh and Bredehoeft, 1981].

**4.1. Estimation of  $c$ -Results**

[37] Talwani and Acree [1984] obtained  $c$  from the temporal and spatial pattern of induced seismicity. They addressed the limitations in the method because of uncertainties in the estimation of  $r$  and  $\Delta t$  and argued that “. . . its main justification lies in the coherent results obtained.” Talwani and Chen [1998] used additional data and recalculated  $c$  from those originally used by them using equation (5). Those and other data and the results are described next.

**4.1.1. From Time Lag Associated With RIS**

[38] There is usually a time lag,  $\Delta t$ , between the start of impoundment of a reservoir and the onset of seismicity or between the start of an increase in lake level and the increase in the seismicity level [Gupta and Rastogi, 1976; Talwani, 1976; Talwani and Acree, 1984]. The time needed for the pore pressure to diffuse from the reservoir to the hypocenters (Figure 2) causes the observed time delay. The observed RIS at Nurek Reservoir, Tadjikistan [Simpson and Negmatullaev, 1981] is a good example where the time lags between water level changes and seismicity were observed. Nurek Reservoir is located in a tectonically active area, where there was seismicity before impoundment. Figure 6 shows the water level changes from 1972 to 1976. The initial filling in July 1972 was followed about 75 days later by an increase in seismicity located about 5 km away. The water level fluctuated between 120 and 140 m from 1973 to early 1976. In June 1976, there was a sudden increase in the water level. This rapid increase in the water level was also followed by an increase in seismicity about 5 km from the reservoir ~50 days later in August 1976. The time lags between water level rise and onset seismicity for the two periods were used to calculate hydraulic diffusivity using equation (5) and yielded values of 0.96 and 1.45  $m^2/s$ , respectively.

[39] Thirty-six values of  $c$  were estimated using the time lag between an increase in water level and RIS using equation (5) (Table 1). The results are given in Table A1. The distance  $r$  was estimated from the deepest part of the reservoir to the hypocenters and ranged between 0.5 and 20 km. The associated time delay ranged from ~2 days to more than 600 days. The errors in estimating these parameters were estimated wherever possible (Table A1). The hydraulic diffusivity values estimated for these 36 cases range between 0.02 and 9.65  $m^2/s$ .

**4.1.2. From Time Lag Between Fluid Injection and Induced Seismicity**

[40] There are many cases where seismicity is associated with fluid injection in deep wells [Healy et al., 1968; Ohtake, 1974; Raleigh et al., 1976; Fletcher and Sykes,

1977; Zoback and Harjes, 1997]. In these cases, high-pressured fluid is injected and the diffusion of the high fluid pressures to the hypocenters induces the seismicity. The time needed for the diffusion of pore pressure causes the observed time lag between the start of injection and the onset of seismicity, and the stopping of the fluid injection can be correlated to the cessation of IIS.

[41] Seismic activity drastically increased at Matsushiro, Japan following the two injections of high-pressured fluid in a 1.8-km deep well in 1970 [Ohtake, 1974]. A time delay of 9.3 days between the start of the first fluid injection and the increase in seismicity and a time delay of 6.2 days between the start of the second injection and the seismicity were observed (Ohtake, 1974, Figure 3). In both cases the seismicity occurred about 3 km from the injection point. Using equation (5) we obtain hydraulic diffusivity values of 2.8 and 4.2  $m^2/s$ , respectively (Table A2).

[42] Ten values of  $c$  were estimated from the time lag between fluid injection (and cessation) and the onset (and cessation) of induced seismicity using equation (5). The distance  $r$  was measured from the injection points to the hypocenters associated with a time delay  $\Delta t$ . The accuracy of the values of  $r$  and  $\Delta t$  were estimated where ever possible (Table A2). The hypocentral distances from the wells for IIS were used as estimates of the distance  $r$ ,

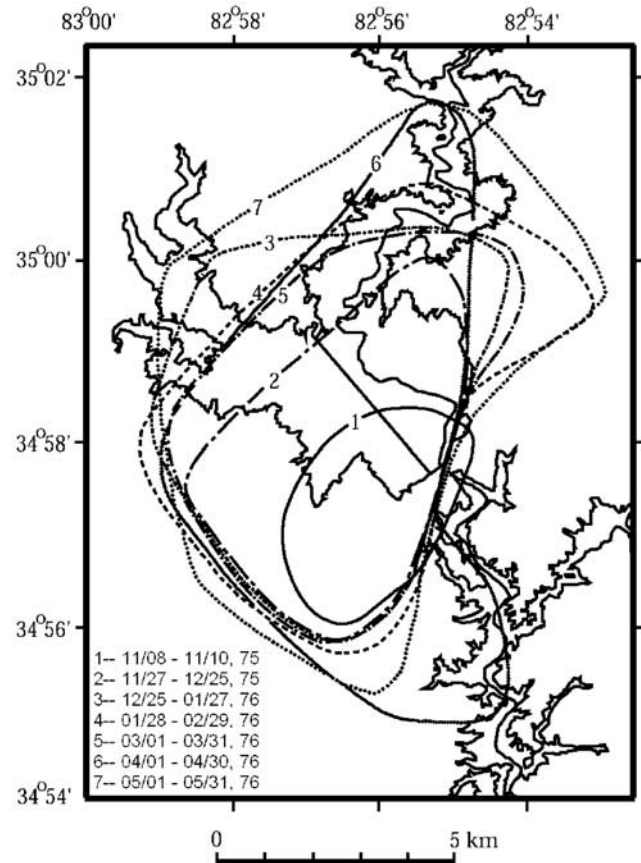


**Figure 7.** Epicentral growth of seismicity at Lake Jocassee, South Carolina from November 1975 to May 1976 (after Talwani and Acree [1984]). The rate of growth was used to calculate  $c$ .

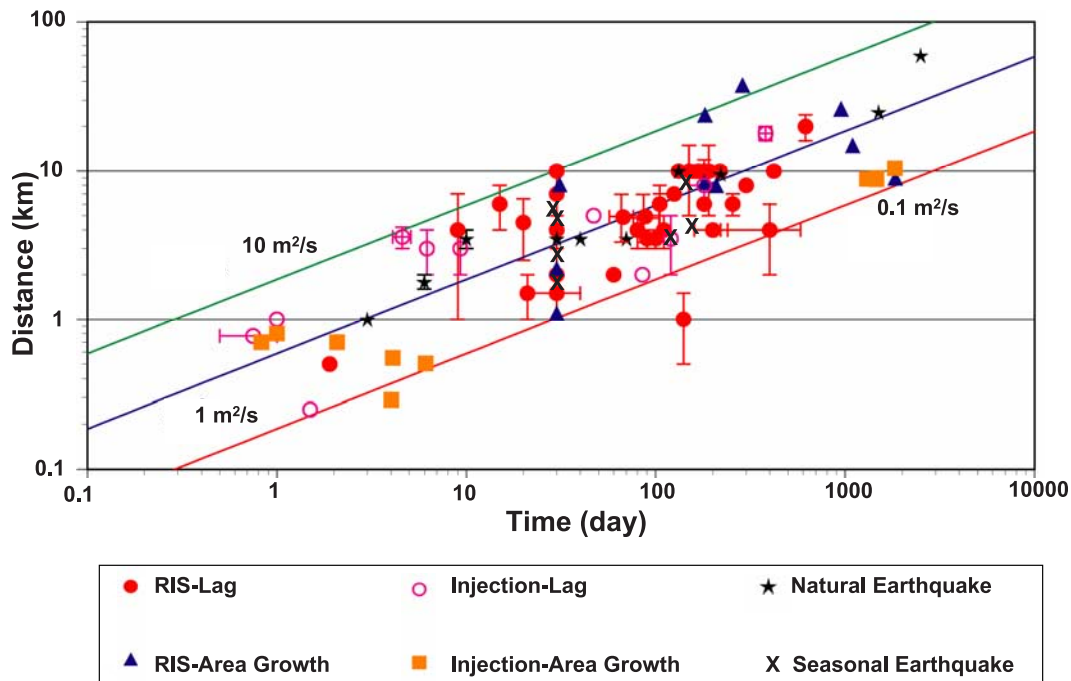


**Figure 8.** Plot showing the observed distance time delay data. RIS lag and injection lag refer to cases where the time lag between filling and seismicity were used to calculate  $c$ . Area growth refer to cases where the rate of epicentral growth was used. Natural earthquakes refer to cases where precursory data were used to calculate  $c$ . Seasonal refers to the cases where a seasonal time lag was used. The parallel lines show hydraulic diffusivity values of 0.1, 1, and  $10 \text{ m}^2/\text{s}$  calculated using equation (5). Virtually, all the diffusivity values lie between 0.1 and  $10 \text{ m}^2/\text{s}$ , a range which is called seismogenic diffusivity  $c_s$ .

and the resulting values of  $c$  range between 0.12 and  $8.33 \text{ m}^2/\text{s}$ .

#### 4.1.3. From the Epicentral Growth of RIS With Time

[43] In some cases we have observed that the pore pressure increase following reservoir impoundment causes a steady temporal expansion of the epicentral area [Talwani, 1981; Talwani and Acree, 1984; Rastogi et al., 1986a]. Figure 7 shows the epicentral distribution with time at Lake Jocassee in northwest South Carolina [Talwani and Acree, 1984]. The seismicity was monitored since the first felt earthquake in the area. The epicentral area was initially in the vicinity of the dam, after which it grew from November 1975 to February 1976, decreased in March 1976 (associated with temporary lowering of the lake level), and then increased again in April and May 1976, when it was the largest. The epicentral area for each month was plotted against time, and its rate of growth was used to determine the hydraulic diffusivity [Talwani and Acree, 1984]. Here the change in the epicentral area in any time  $\Delta t$  was used instead of  $r^2$  in equation (5). Ten values of  $c$  were obtained by this method, ranging from 0.13 to  $12.33 \text{ m}^2/\text{s}$  (Table A3).

#### 4.1.4. From the Epicentral Growth of Fluid-Injection-Induced Seismicity

[44] In fluid injection experiments and geothermal and oilfield exploitation, the fluid pressure front grows with time. This phenomenon was observed in Cogdell Oil Field, Texas [Davis and Pennington, 1989], the KTB experiment [Shapiro et al., 1997], Hijiori fluid injection experiment [Sasaki, 1998], and Soultz and Ogachi fluid injection experiments [Audigane et al., 2000]. From the aerial growth

in the 250-bar fluid pressure contours in the Cogdell oil field between 1970 and 1983 (where fluids were injected at high pressures to recover oil, [Davis and Pennington, 1989, Figure 7]) and the associated seismicity from November 1974 to 1983, the hydraulic diffusivity was found to be  $0.15 \text{ m}^2/\text{s}$ . Nine values of  $c$  were obtained by this method and ranged between 0.08 and  $1.85 \text{ m}^2/\text{s}$  (Table A4).

#### 4.1.5. From the Duration of Precursors

[45] In the study of earthquake precursors in the early 1970s, it was observed that the duration of various precursory changes, which were attributed to fluid pressure diffusion, was related to the magnitude of the earthquake [Anderson and Whitcomb, 1973; Scholz et al., 1973; Whitcomb et al., 1973]. The magnitude was proportional to a characteristic dimension, which was estimated from the aftershock area of larger earthquakes, and from an empirical relationship between the fault length and magnitude [Whitcomb et al., 1973]. Scholz et al. [1973] presented a figure showing a linear relationship between the precursor time interval for an earthquake and the length of its aftershock zone. We took their data and calculated the hydraulic diffusivity using equation (5), with  $r$  equal to the length of the aftershock zone and  $\Delta t$  is the precursory time interval (the time for the diffusion of pore pressure). Ten values of  $c$  ranging from 0.66 and  $4.17 \text{ m}^2/\text{s}$  were obtained by using these data (Table A5).

#### 4.1.6. From Time Lag Associated With Seasonal Seismicity

[46] Several recent studies have shown an association between precipitation and seismicity. For example, Ventura and Vilardo [1999] observed a 4 month delay between the

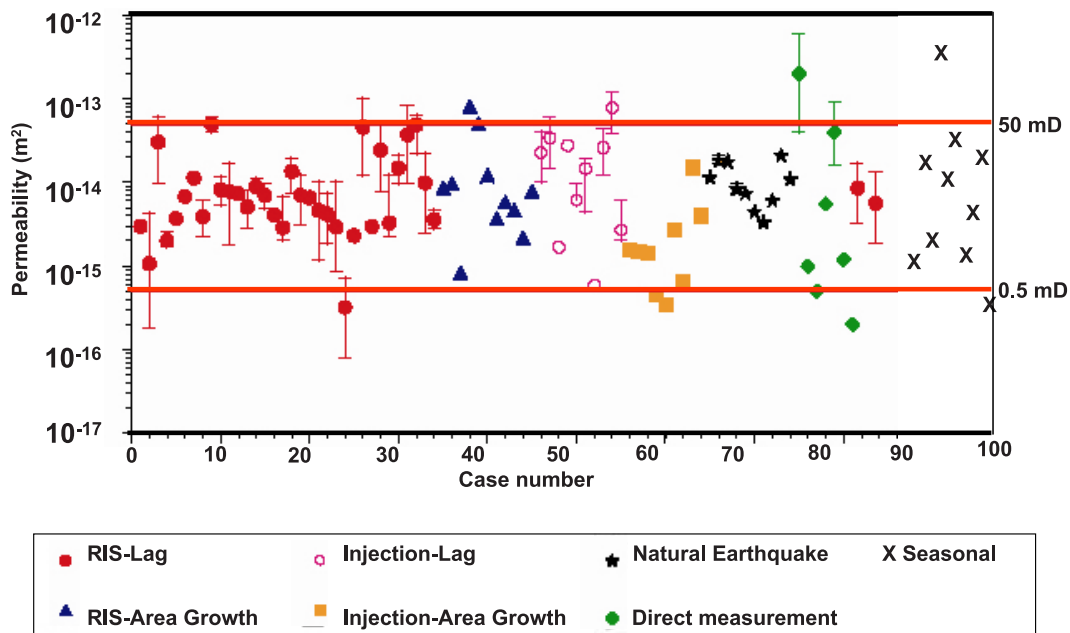


**Figure 9.** Results of the calculation of intrinsic permeability  $k$  using values of  $c$  shown in Figure 8 and equation (6), and six direct measurements at locations of induced seismicity. The symbols are the same as were used in Figure 8. The permeability of fractures associated with seismicity lies between  $5 \times 10^{-16}$  and  $5 \times 10^{-14} \text{ m}^2$ . This range has been labeled seismogenic permeability,  $k_s$ .

seasonal rainfall maxima and the annual peak in seismicity, whereas *Ogasawara et al.* [2002] estimated a diffusivity value of  $\sim 0.1 \text{ m}^2/\text{s}$  based on an association between periods of heavy rainfall and shallow low-level microseismicity in an abandoned, flooded Ikuno mine in Japan. In a focused experiment, *Kraft et al.* [2005] calculated  $c \sim 1 \text{ m}^2/\text{s}$  based on a careful association of well-recorded rainfall and seismicity data at Mt. Hochstaufen in southeastern Germany. An improved estimate of  $3.3 \pm 0.8 \text{ m}^2/\text{s}$  was obtained by *Hainzl et al.* [2006] (Table A6).

[47] *Wolf et al.* [1997] have documented a correlation between a seasonal pattern in seismicity and groundwater recharge due to snowmelt. *Saar and Manga* [2003] showed that some seismicity at Mt. Hood, Oregon, occurring at a depth of about 4.5 km, was triggered by pore pressure diffusion as a result of a rapid groundwater recharge due to a seasonal snowmelt, with a statistically significant time lag of 151 days. From these data they estimated a hydraulic diffusivity to be  $0.30 \pm 0.22 \text{ m}^2/\text{s}$ . *Christiansen et al.* [2005] extended the Mt. Hood study and established a seasonal pattern of seismicity at five volcanic centers in western United States where adequate seismicity and precipitation data were available. The results of estimating  $c$  from “seasonal” seismicity are presented in Table A6. Ten of the 11 values lie in the range between 0.1 and  $10.0 \text{ m}^2/\text{s}$ , with an outlier at  $13.5 \text{ m}^2/\text{s}$ . However, using equation (5), this anomalous value reduces to  $3.5 \text{ m}^2/\text{s}$ . These values are order of magnitude estimates because of large uncertainties in the exact time of commencement of pore pressure diffusion and in hypocentral depths.

#### 4.1.7. From Direct Measurements

[48] Hydraulic diffusivity of seismogenic fractures was obtained from direct measurements of two hydrologic parameters at wastewater injection sites in Denver, Colorado

and northeastern, Ohio. At each of these sites, the transmissivity  $T$  and the storativity  $S$  were obtained by injection and pumping tests [*Hsieh and Bredehoft*, 1981; *Nicholson et al.*, 1988]. The hydraulic diffusivity was calculated from the relation  $c = T/S$ . It was found to be 1.1 and  $0.2 \text{ m}^2/\text{s}$ , respectively (Table A7).

#### 4.1.8. Results of Estimation of $c$

[49] Estimates of  $c$  obtained by different methods are given in Appendix A. The corresponding time and distance values have been plotted on a log-log scale (Figure 8). The error bars for the distance  $r$  and the time lag  $\Delta t$  for those points where they could be estimated have also been plotted in Figure 8. The three parallel lines represent values of  $c$  equal to 0.1, 1.0, and  $10 \text{ m}^2/\text{s}$ . From the figure, and the data given in Appendix A, we note that 84 of the 88 data points lie in the range 0.1 to  $10.0 \text{ m}^2/\text{s}$  (Table 1). In one case,  $c = 12.3 \text{ m}^2/\text{s}$  was associated with the epicentral growth at Koyna Reservoir for the 4 month period following the December 1967 M6.3 earthquake. Other estimates for Koyna range between 0.1 and  $1.7 \text{ m}^2/\text{s}$ . Of the two low values ( $< 0.1 \text{ m}^2/\text{s}$ ), one ( $0.08 \text{ m}^2/\text{s}$ ) was estimated from the epicentral growth at a hot dry rock site at Soultz, France, where the injection pressure exceeded the hydrostatic [*Audigane et al.*, 2000]. At Hunanzhen Reservoir, China,  $c \sim 0.02 \text{ m}^2/\text{s}$  was estimated from a long lag time (167 days) for seismicity 1 km from the reservoir, (this long delay could be associated with chemical weakening in this predominantly karst region). *Roeloffs* [1996, Figure 14, p. 168] has shown that, in nature, there is a wide range of values of  $c$ , from  $10^{-12}$  to  $10^4 \text{ m}^2/\text{s}$ . Here we find that for 94 % of the cases, where the seismicity is associated with pore pressure diffusion, the hydraulic diffusivity of the seismogenic fractures varies over only 2 orders of magnitude, 0.1 to  $10.0 \text{ m}^2/\text{s}$ . We conclude that this range is a

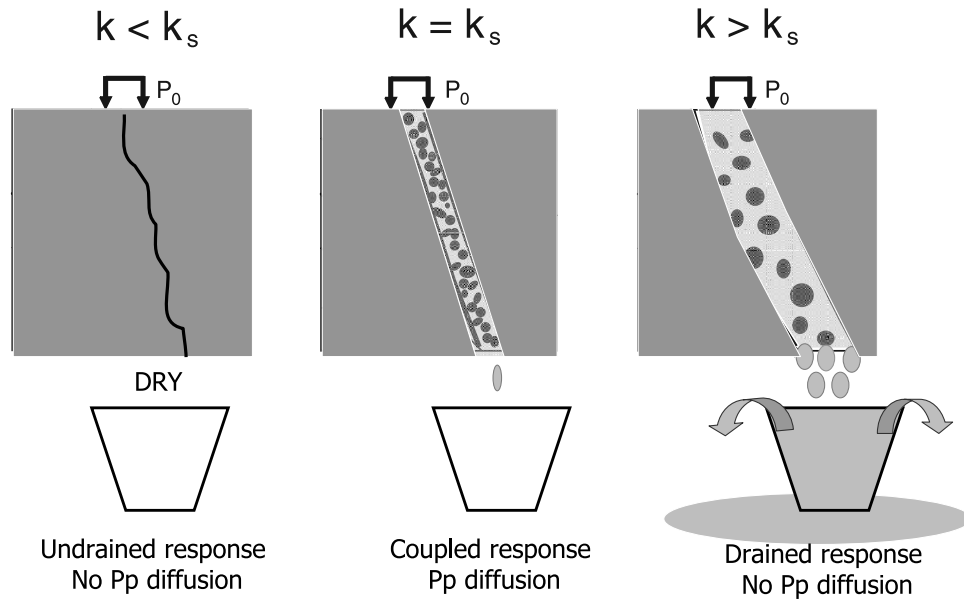


**Figure 10.** Cartoon to explain the consequences of loading a fracture with permeability  $k$ , where  $k$  is less than, equal, and greater than  $k_s$ .

characteristic value for seismogenic fractures where the seismicity is associated with the diffusion of fluid pressures at normal crustal temperatures. We label it seismogenic diffusivity  $c_s$ .

## 5. Estimation of the Intrinsic Permeability, $k$

[50] The fracture permeability  $k$  is related to hydraulic diffusivity  $c$  by

$$k = c\mu\{\Phi\beta_f + (1 - \Phi)\beta_r\} \quad (6)$$

where  $\mu$  is the viscosity of water,  $\Phi$  is porosity, and  $\beta_f$  and  $\beta_r$  are the compressibilities of water and rocks, respectively [Bodvarsson, 1970]. The following typical values of these parameters are used in calculating permeabilities from the estimated values of hydraulic diffusivities using equation (6),  $\Phi = 3 \times 10^{-3}$ ,  $\beta_f = 10^{-10} \text{ Pa}^{-1}$ , and  $\beta_r = 2 \times 10^{-11} \text{ Pa}^{-1}$  [Talwani et al., 1999].

[51] In earlier studies the value of the viscosity of water at  $20^\circ\text{C}$ ,  $10^{-3} \text{ Pa s}$ , was assumed for all calculations [e.g., Scholz et al., 1973; Brace, 1980; Talwani and Acree, 1984]. However, the viscosity of water decreases rapidly with increasing temperature [Weast, 1987]. Therefore, in calculating  $k$  from the values of  $c$  obtained in the last section, we estimated the viscosity as a function of depth. Assuming an average thermal gradient of  $30^\circ\text{C}/\text{km}$  [Lillie, 1999], we obtained a plot of the viscosity of water as a function of depth, using the viscosity versus temperature data from the work of Weast [1987]. The viscosity value decreased from  $10^{-3} \text{ Pa s}$  at the surface to  $10^{-4} \text{ Pa s}$  at a depth of 8 km. While using equation (6) to calculate  $k$ , we used the viscosity value corresponding to half the hypocentral depth as an estimate for the representative viscosity.

[52] Figure 9 shows the calculated permeability values from the diffusivity data together with an additional six directly measured values at locations of induced seismicity (Table A8). The two horizontal lines represent permeability

values of  $5 \times 10^{-16}$  and  $5 \times 10^{-14} \text{ m}^2$  (0.5 and 50 mD), respectively. From Figure 9 we note that 86 of the 93 data points (92%) lie between of  $5 \times 10^{-16}$  and  $5 \times 10^{-14} \text{ m}^2$ .

[53] Permeability values of crystalline rocks compiled by Brace [1980] and Clauser [1992] all showed a variation of more than 10 orders of magnitude. Measurement of permeability values of the oceanic crust also yielded a similar variation [Fisher, 1998]. This large variation is scale dependent, with low values for laboratory samples (a few centimeters) to in situ crustal values. Towend and Zoback [2000] showed that, on a crustal scale, permeability values range between of  $10^{-20}$  and  $>10^{-17} \text{ m}^2$ . Crustal permeabilities  $\sim 10^{-13} \text{ m}^2$  were obtained following the Kobe earthquake [Kitagawa et al., 1999], suggesting that in situ crustal permeabilities can range over 7 orders of magnitude.

[54] The permeability values from seismicity areas obtained in this study lie in a narrow range compared to those in nature. This narrow range is characteristic of the fractured rocks where fluid pressure diffusion is associated with seismicity and has been labeled as the seismogenic permeability  $k_s$  [Talwani and Chen, 1998].

## 6. Discussion

[55] Induced seismicity is associated with fluid pressure diffusion through discrete fractures and not with the bulk of the rock mass. Fluid (and fluid pressure) flow does not occur along a plane perpendicular to the least principal stress, but in a few preexisting fractures [Cornet and Yin, 1995]. Our data suggest that seismogenic permeability  $k_s$  is an intrinsic property of the fractures associated with seismicity. Whereas crustal permeability of rocks varies over 7 orders of magnitude,  $k_s$  lies between  $\sim 5 \times 10^{-16}$  and  $5 \times 10^{-14} \text{ m}^2$ .

[56] In one of the earlier attempts to study the flow of fluids through fractures, Sharp and Maini [1972] carried out flow tests between synthetic, parallel fractures with four increasing “effective” openings. From the results of

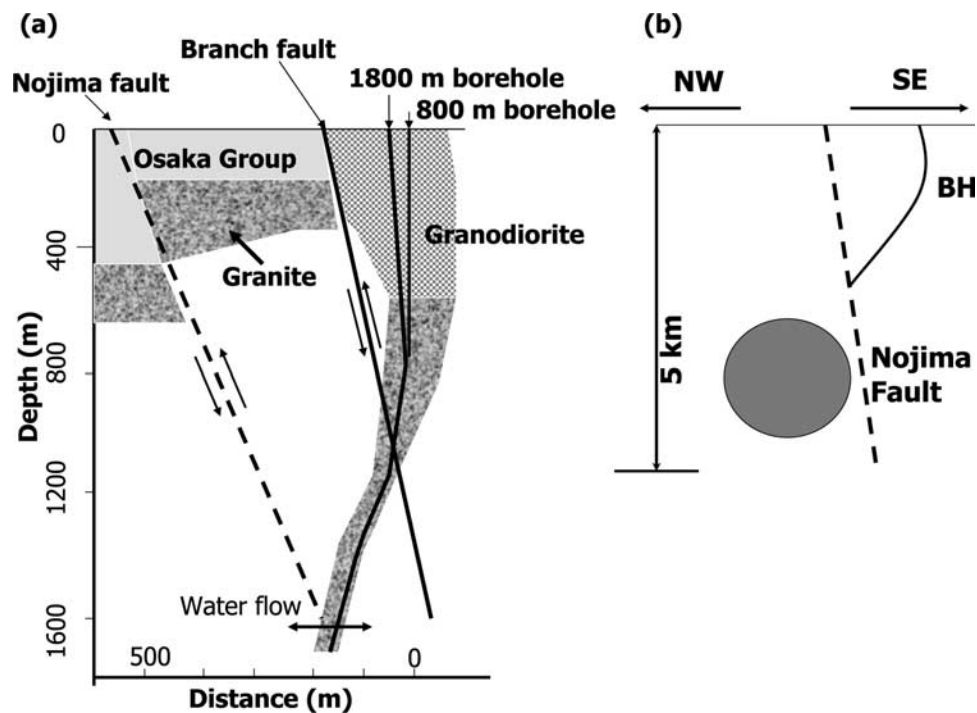


**Figure 11.** (a) Geometry of three boreholes drilled near Nojima fault, and (b) the location of seismicity. The 800-m deep well was artesian and showed correlative changes in discharge with episodes of fluid injection in the deep well. Seismicity (shaded circle) was located off the fault and followed injection episodes after a few days (Figure 11b). See text for details (modified from the work of *Murakami et al.* [2001] and *Tadokoro et al.* [2000]).

these experiments they found that, as the openings increased, they “observed that a limited range of linear flow occurred followed by a nonlinear range which finally gave way to fully turbulent conditions. The transition between flow states was found to be smooth.” They further concluded that the permeability of fractures is sensitive to pressure changes. Conversely, pore pressure changes in fractures, associated with fluid flow are dependent on their permeability.

[57] We illustrate how the permeability of the fracture affects pore pressure changes by examining three cases, where the fracture permeability  $k$  is less than, equal to, and greater than the seismogenic permeability  $k_s$  (Figure 10). An increase in pressure at one end of the fracture, for example, by an increase in lake level, results in diffusion of pore pressure (undrained response) and fluid flow (drained response) through the fracture. The rate of increase in pore pressure,  $dp/dt$ , and the rate of fluid flow determine if the fractures will be seismogenic or not. An increase in  $dp/dt$  leads to delayed seismicity, whereas an increase in fluid flow rates lowers  $dp/dt$ , and results in an absence of seismicity. These effects tend to be more pronounced for rapid filling rates and muted for slower filling.

[58] For rocks with permeability  $k < k_s$ , there is a great resistance to the flow of water through the fracture and there is a negligible pore pressure increase by diffusion. In equation (3), as  $c \rightarrow 0$ , the second term is zero and  $p(r, t) \rightarrow \alpha$ . The rocks respond elastically, and any increase in pore pressure away from the reservoir is instantaneous and due to Skempton’s effect (2) (Figure 10). For fractures with  $k < k_s$ , the application of very large differential pressures can cause

the fractures to open, thereby increasing the value of  $k$  to  $k_s$  and triggering seismicity.

[59] For rocks with permeability  $k > k_s$ , as  $c \rightarrow \infty$ , there is a drained response, the fluid flow is non-Darcian, with a large fluid flow gradient which reduces the growth rate of  $dp/dt$ , and results in no seismicity. In this case, equation (3), which is based on the assumption of the Darcian flow, does not apply. In the special case encountered in fluid injection experiments, the pore pressure is large enough to keep the fractures open, and slightly greater than the normal stress acting at the surface, so there is no shear component acting on the surface, and hence, no seismicity.

[60] The amount of fluid flow through the fractures can be obtained by assuming flow in parallel vertical cracks. For one-dimensional flow between parallel cracks, *Kohl et al.* [1997] found a flow rate per unit height of a vertical fracture to be  $0.017 \text{ L s}^{-1} \text{ m}^{-1}$  ( $1.47 \text{ m}^3 \text{ d}^{-1} \text{ m}^{-1}$ ) at the onset of nonlinear (non-Darcian) flow, i.e., when the fracture permeability  $k$  just exceeded  $k_s$ . The flow rate was about 20 times larger for turbulent flow and 2 orders of magnitude lesser for linear flow, i.e., when  $k = k_s$ .

### 6.1. Insights From Injection-Induced Seismicity

[61] Our understanding of seismogenic permeability can provide insight into the behavior of fractures associated with fluid-induced seismicity. Figure 1, modified from the work of *Tezuka and Niitsuma* [2000], shows a fluid-filled fracture subjected to a two-dimensional stress field with  $\sigma_1$  and  $\sigma_3$  being the maximum and minimum principle stresses, respectively, with the intermediate stress  $\sigma_2$  normal to the plane of the paper. The fracture plane is oriented at an angle

**Table A1.** Estimation of  $c$  From Time Lag of RIS

Location	Start of Water Level Increase	Earthquake Date	Time Lag, Day	Distance, km	$c$ , m <sup>2</sup> /s	Errors		Reference
						Time	Distance	
Oued Fodda, Algeria	December 1932	January 1933	30	2	0.58			<i>Gupta and Rastogi</i> [1976]
Mead, USA	May 1935	1937	400	4	0.12	2	180	<i>Carder</i> [1945]
Xinfengjiang, China	20 October 1959	November 1959	30	7	4.73	3		<i>Ding</i> [1987]
Vajont, Italy	January 1960	July 1960	200	4	0.23	40		<i>Gupta and Rastogi</i> [1976]
Kurobe, Japan	October 1960	August 1961	300	8	0.62			<i>Gupta and Rastogi</i> [1976]
Mendocino, USA	01 November 1961	06 June 1962	218	10	1.33			<i>Topozada and Cramer</i> [1978]
	15 November 1977	26 March 1978	132	10	2.19			
Monteynard, France	November 1961	25 April 1962	110	4	0.42	1		<i>Grasso et al.</i> [1992]
	22 October 1979	22 November 1979	30	10	9.65			
Kariba, Zambia	January 1963	July 1963	180	10	1.61	2		<i>Pavlin and Langston</i> [1983]
Kremasta, Greece	12 July 1965	05 February 1966	190	10	1.52	5	10	<i>Gupta and Rastogi</i> [1976]
Bajina, Basta	15 March 1967	03 July 1967	125	7	1.13			<i>Gupta and Rastogi</i> [1976]
Koyna, India	26 June 1967	13 September 1967	80	4	0.58	1	1	<i>Gupta and Rastogi</i> [1976]
	26 June 1967	10 December 1967	168	10	1.72	1		
	05 July 1973	01 October 1973	105	6	0.99			
Hendrik Ver Woerd, South Africa	01 September 1970	27 December 1971	180	6	0.58			<i>Gupta and Rastogi</i> [1976]
Zhelin, China	31 January 1971	24 October 1972	255	6	0.41	1		<i>Huang and Kong</i> [1984]
Tabingo, Australia	01 May 1971	01 June 1971	30	4	1.54	1		<i>Gupta and Rastogi</i> [1976]
Nurek, Tajikistan	July 1972	October 1972	90	5	0.96	2	10	<i>Simpson and Negmatullaev</i> [1981]
	June 1976	August 1976	60	5	1.45	2	10	
Shenwo, China	01 November 1972	February 1973	105	6	0.99	2		<i>Zhong et al.</i> [1995]
Clark Hill, USA	13 March 1975	15 March 1975	1.9	0.5	0.38			<i>Talwani</i> [1976]
Manic3, Canada	August 1975	September 1975	30	2	0.39	1		<i>Leblanc and Anglin</i> [1978]
Monticello, USA	03 December 1977	25 December 1977	21	1.5	0.31	0.5		<i>Talwani and Acree</i> [1987]
LG2, Canada	27 November 1978	27 December 1978	30	1.5	0.22	0.5	10	<i>Anglin and Buchbinder</i> [1985]
Hunanzhen, China	12 January 1979	28 June 1979	140	1	0.02	0.5		<i>Hu et al.</i> [1986]
LG3, Canada	12 April 1981	June 1981	60	2	0.19			<i>Anglin and Buchbinder</i> [1985]
Dahua, China	27 May 1982	04 June 1982	9	4	5.14	3		<i>Guang</i> [1995]
Srinamsagar India	January 1983	June 1984	420	10	0.58			<i>Rastogi et al.</i> [1986b]
Khao Laem, Thailand	June 1984	July 1984	20	4.5	2.93	2		<i>Mahasandana and Pinrode</i> [1995]
Dongjiang, China	02 August 1986	November 1986	100	3.5	0.35	0.5	5	<i>Hu et al.</i> [1995]
Rajjaprabha, Thailand	01 October 1986	10 June 1988	618	20	1.87	4		<i>Klaipongpan and Chitrakarn</i> [1995]
Yantan, China	19 March 1992	29 March 1992	9	4	4.21	3		<i>Guang</i> [1995]
Warna, India	July 1993	August 1993	15	6	6.94	2		<i>Rastogi et al.</i> [1997a]
Tarbela			150	10	1.92	5		<i>Ali</i> [1989]
Açu			90	3.5	0.39	0.5		<i>Ferreira et al.</i> [1995]

Columns 2, 3, 4, 5, and 7 are from the corresponding references, and column 6 is calculated using equation (5).

$\theta$  with respect to  $\sigma_3$ , with the pore pressure  $p$ . *Townend and Zoback* [2000] provided evidence of nearly hydrostatic fluid pressures at depths of several kilometers at various locations. Increase in  $p$  leads to failure in accordance with the Coulomb failure criterion (1).

[62] In the 1990s greater insight in to the nature of fluid flow through fractures was obtained when fluids were injected in experimental wells. Studies of injection-induced

seismicity, where fluid pressure information is available, provide quantitative data to illustrate the ideas presented earlier. At hot dry rock sites and other locations of IIS, the behavior of fractures depends on both the injection rates and on the differential pressures (downhole wellbore pressure excess over the ambient natural pressures [*Evans et al.*, 2005]).

**Table A2.** Estimation of  $c$  From Time Lag of Fluid Injection Seismicity

Location	Start of Injection	Onset of Seismicity	Time Lag, Day	Distance, km	$c$ , m <sup>2</sup> /s	Uncertainty		Reference
						Time	Distance	
Denver, USA	08 March 1962	24 April 1962	47	5	1.54			<i>Healy et al.</i> [1968]
Matsushiro, Japan	15 January 1970	25 January 1970	9.3	3	2.80		1	<i>Ohtake</i> [1974]
	31 January 1970	06 February 1970	6.2	3	4.20			
Dale, USA	03 August 1971	28 October 1971	85	2	0.14			<i>Fletcher and Sykes</i> [1977]
Rangely, USA			1	1	2.89 <sup>a</sup>			<i>Raleigh et al.</i> [1976]
El Dorado, USA	Middle 1983	09 December 1983	180	8	1.03	30	2	<i>Cox</i> [1991]
	Late 1987	Early 1989	380	18	2.47	30	2	
KTB, Germany			1.5	0.25	0.12 <sup>b</sup>			<i>Kessels and Kück</i> [1995]
Nojima, Japan			0.75	0.88	2.99 <sup>c</sup>	0.25		<i>Kitagawa et al.</i> [1999]
			4.5	3.5	7.8 <sup>c</sup>	0.5	0.5	<i>Tadokoro et al.</i> [2000]

The columns 2, 3, 4, 5, and 7 are from the corresponding references, and the column 6 is calculated using equation (5).

<sup>a</sup> $c$  is estimated using the time lag between injection water back flow and cessation of earthquake.

<sup>b</sup> $c$  is estimated from the fluid communication of two wells at 4 km deep. Authors provide time lag and distance.

<sup>c</sup> $c$  is estimated from the relation between fluid injection in deep well and water discharge in an observation well.

**Table A3.** Estimation of  $c$  From Epicentral Area Growth of RIS

Location	Time Period	Time Duration, Days	Area Growth, km <sup>2</sup>	$c$ , m <sup>2</sup> /s	Reference
Xinfengjiang, China	October 1959–18 March 1962	900	416	1.35	<i>Wang et al.</i> [1976], <i>Talwani</i> [1981]
	19 March 1962–31 December 1962	287	150	1.53	
Koyna, India	June 1962–13 July 1967	1837	80	0.13	<i>Talwani</i> [1981]
	11 October 1967–10 April 1968	182	590	12.48	
Oroville, USA	01 August 1975–01 September 1975	31	67	6.28	<i>Talwani</i> [1981], <i>Lester et al.</i> [1975]
Jocassee, USA	06 November 1975–31 May 1976	208	65	0.89	<i>Talwani</i> [1981], <i>Talwani and Acree</i> [1984]
Dhamni, India	August 1994–September 1994	30	5	0.47	<i>Rastogi et al.</i> [1997b]
Kariba, Zambia	January 1962–June 1962	180	70	1.13	<i>Gough and Gough</i> [1970]
Nurek, USSR	July 1972–June 1975	1095	225	0.59	<i>Soboleva and Mamadaliev</i> [1976]
Bhatsa, India	1983–1984	30	1.3	0.16	<i>Rastogi et al.</i> [1986a] <sup>a</sup>

Columns 2, 3, and 4 are from the corresponding references, and column 5 was calculated using equation (5).

<sup>a</sup>Author calculated growth rate.

[63] Injections at very high differential pressures ( $p \gg \sigma_3$ ) result in tensile opening of fractures, or “jacking” near the borehole, with shearing occurring farther out, and diffusion of fluid pressure into the unstimulated fractures still farther away [*Pine and Batchelor*, 1984].

[64] Jacking results in the widening of fracture apertures, an increase in permeability to values  $>k_s$ , increases fluid flow, and results in an absence of seismicity. An increase in permeability to values  $>k_s$  can also result from the opening of fractures following an earthquake, as was observed, for example, following the Loma Prieta earthquake [*Rojstaczer et al.*, 1995].

[65] *Tezuka and Niitsuma* [2000] have shown that, in the case of injection-induced seismicity, slip occurs when the total pore pressure is a fraction of  $\sigma_3$  and its initiation depends on the orientation of the fractures with respect to  $\sigma_3$ . When the pore pressure remains less than  $2/3 \sigma_3$ , the hydrologic system responds linearly and Darcy’s law applies [*Cornet and Morin*, 1997], and fluid pressure growth can be described by the diffusion equation. The shear deformation is associated with a large seismic energy release, and the regions of injection-induced seismicity represent zones of increased pore pressures and not increased fluid flow [*Cornet and Yin*, 1995].

[66] When the fluid pressures exceed  $\sigma_3$ , tensile fractures open up and the new permeability exceeds  $k_s$ . In fractures where the permeability has been changed to exceed  $k_s$ , or in naturally occurring rocks with  $k > k_s$ , the fluid flow is non-Darcian and can be approximated by flow through parallel plates [*Cornet*, 2000]. The pore pressure changes are insignificant compared to values predicted by the assump-

tion of Darcy flow [*Cornet*, 2000] and are derived from the application of the diffusion equation (3). That is, in the drained conditions that result from  $k > k_s$ , there are no fluid pressure increases. *Kohl et al.* [1997] showed that the equation for pore pressure diffusion

$$\frac{\partial p}{\partial t} = \frac{1}{S_s} \nabla \cdot (K \cdot \nabla p) \quad (7)$$

for Darcian flow should be modified to

$$\frac{\partial p}{\partial t} = \frac{1}{S_s} \nabla \cdot [\bar{K} \cdot (\nabla p)^{1/2}] \quad (8)$$

for non-Darcian flow, where  $S_s$  is the specific storage coefficient,  $K$  is the hydraulic conductivity and  $\bar{K}$  is a function of the ratio of relative roughness and aperture of the fractures and fluid density (see *Kohl et al.* [1997] for details). Thus equation (3) which was based on the assumption of Darcian flow would have to be amended for  $k > k_s$  or for  $c > c_s$ . Hence the curves showing changes in pore pressure  $p$  and  $dp/dt$  (Figures 3 and 4) for  $c > 10 \text{ m}^2/\text{s}$  would have to be modified. *Kohl et al.* [1997] found that their analyses of flow data suggested that nonlaminar flow may be common to fracture flow in moderate to high flow rates within Soultz and perhaps in other fractured reservoirs.

[67] From these observations, we conclude that in locations of geothermal, volcanic reservoir- and injection-induced seismicity, the application of small differential pressures results in seismicity in fractures with  $k_s$  and aseismic fluid flow in fractures whose permeability

**Table A4.** Estimation of  $c$  From Epicentral Area Growth of Fluid Injection Seismicity

Location	Time Period	Time Duration, Day	Area Growth, km <sup>2</sup>	$c$ , m <sup>2</sup> /s	Reference
Cogdell Oil Field, USA	1970–1975	1825	110	0.16	<i>Davis and Pennington</i> [1989]
	1975–1979	1460	79	0.15	
	1979–1983	1460	77	0.15	
Soultz, France	October 1993	6.25	0.25	0.11	<i>Audigane et al.</i> [2000]
	June 1995	4.17	0.12	0.08	
	September 1996	2.08	0.49	0.68	
Ogachi, Japan	1989	2.67	0.32	0.35	<i>Audigane et al.</i> [2000]
Hijiori, Japan	1988–1989	1	0.63	1.85	<i>Sasaki</i> [1998]
KTB, Germany		0.83	0.49	1.7	<i>Zoback and Harjes</i> [1997]

Columns 2, 3, and 4 are from the corresponding references, and the column 5 is calculated using equation (5).

**Table A5.** Estimation of  $c$  From Duration of Precursors

Location	Precursor Time, Day	Length of Aftershock Zone, km	$c$ , m <sup>2</sup> /s	Uncertainty	
				Time	Distance
BML, USA	3	1	0.96		
	6	1.8	1.56		0.2
Tashkent, Former USSR	10	3.5	3.54		
	175	10	1.65	25	0.5
Danville, USA	30	3.5	1.18		
Garm, Former USSR	40	3.5	0.89		
	70	3.5	0.66		
San Fernando, USA	1500	25	1.21		
Niigata, Japan	2500	60	4.17		
	132	10	2.19		

Columns 2, 3, and 5 are from the work of *Scholz et al.* [1973]. Column 4 is calculated using equation (5).

exceeds  $k_s$ . We illustrate the validity of these conclusions with three examples of IIS.

### 6.2. Nojima Fault Zone

[68] Following the 1995 M7.2, Kobe, Japan earthquake, a drilling program was carried out at the Nojima Fault Zone. The granitic rocks (granite and granodiorite) are faulted at depth and are in fault contact with a sedimentary layer (Osaka group) at the surface [*Murakami et al.*, 2001]. Three wells were drilled to depths of 500, 1800, and 800 m; the former two intersecting the Nojima Fault which had ruptured during the 1995 earthquake (Figure 11a). The third was drilled vertically into the hanging wall of the Nojima Fault. It had an open interval between 785 and 791 m that lay within a granitic bedrock [*Kitagawa et al.*, 1999]. This borehole was an artesian well. The discharge data were recorded every minute. In February and March 1997, large volumes of water were injected at depths between 1480 and 1670 m in the deep hole at differential pressures of 6 to 7 MPa. Changes in discharge were noted in the artesian well 1, 0.5, and 0.5 days following three episodes of injection, respectively. No seismicity was observed between the two wells. Assuming fluid flow, *Kitagawa et al.* [1999] estimated the permeability of the fault zone and surrounding fractures to be  $8 \times 10^{-14}$  to  $4 \times 10^{-13}$  m<sup>2</sup>, values greater than  $k_s$ . However, 4 to 5 days after each injection, seismicity was observed away from the fault, at distances from 3 to 4 km from the location of fluid injection (*Tadokoro et al.*, 2000; Figure 11b). On the basis of the time lag between the time of injection and the onset of seismicity, the authors estimated the permeability of the region (fractures?) connecting the injection point with hypocenters to be  $10^{-15}$  to  $10^{-14}$  m<sup>2</sup>, i.e.,  $\sim k_s$ .

[69] These observations are consistent with our concept of  $k_s$ . Injection of fluids with a borehole pressure of

$\sim 22$  MPa at a depth with hydrostatic pressure  $\sim 15$  MPa caused an increase in pore pressure in the surrounding rocks. There was no seismicity in the Nojima Fault Zone and the surrounding fractures above the injection location where the permeability was greater than  $k_s$ . However, seismicity was observed in fractures with seismogenic permeability adjacent to the fault and below the location of injection.

### 6.3. Le Mayet de Montagne Granite Test Site

[70] The Le Mayet de Montagne granite test site in central France was the location of large-scale in situ experiments involving forced water circulation between two vertical boreholes 100 m apart [*Scotti and Cornet*, 1994]. The boreholes were located in a 1 km<sup>3</sup> block of “fairly homogeneous” granite and reached depths of 780 and 840 m. In the deeper borehole, *Scotti and Cornet* [1994] and *Cornet and Yin* [1995] discovered that increases in injection pressures resulted in increased fluid flow, aseismic widening and slip of a fault cut by the borehole, and triggering of seismicity in a nonparallel (to the fault) set of orthogonal fractures. We interpret these observations to suggest that, following injection, the elevated fluid pressures caused jacking of the fractures in the fault zone, causing aseismic slip and an increased flow in the fault with  $k > k_s$ , and seismicity in the adjacent fractures with seismogenic permeability.

### 6.4. Soultz Hot Dry Rock Site

[71] At the HDR site near Soultz, injection of fluids in September 1993 at a depth of 2850 m triggered seismicity [*Cornet et al.*, 1997]. *Evans et al.* [2005] noted that the rock permeability was initially very low ( $1.5 \times 10^{-17}$  m<sup>2</sup>, i.e.,  $< k_s$ ), but rapidly increased after the differential pressure rose above 5 MPa, and the first microseismic events were observed. By the end of the 6 L s<sup>-1</sup> fluid injection rate stage, there was a 200-fold increase in the transmissivity and the permeability increased to the seismogenic permeability range. This increase in the permeability to the seismogenic permeability value was accompanied by a dramatic increase in seismicity. Further increase in the flow rate to differential pressures of 8.4 to 8.9 MPa were accompanied by a decrease in seismicity and a permanent opening of fractures. The differential pressure stabilized at  $\sim 9$  MPa; that is, there was no further increase in differential pressure even when the flow rates were increased [*Evans et al.*, 2005]. Re-injection in 1994 at 1 MPa differential pressure revealed that the fractures had opened permanently by jacking in 1993. We interpret this observation to mean that the new permeability of the fractures exceeded  $k_s$ . The injectivity, defined as flow rate per unit differential pressure, increased from 0.6 L s<sup>-1</sup> MPa<sup>-1</sup> to 9.0 L s<sup>-1</sup> MPa<sup>-1</sup> [*Evans et al.*, 2005]

**Table A6.** Estimation of  $c$  From Time Lag Between Intense Rainfall and Seismicity

Location	Time Lag, Days	Distance, km	$c$ , (m <sup>2</sup> /s)	Reference
Ikuno Mine, Japan	<20	0.5–1.25	>0.04–0.23 $\sim$ 0.1	<i>Ogasawara et al.</i> [2002]
Swiss Alps	30–60	1–10	0.1–4.8 $\sim$ 1.0	<i>Roth et al.</i> [1992]
Vesuvius, Italy	120	3.5 $\pm$ 1.5	0.30	<i>Ventura and Vilaro</i> [1999]
Mt. Hochstaufen, SE Germany	Variable	1–4	0.75 $\pm$ 0.35 <sup>a</sup>	<i>Kraft et al.</i> [2005]
Mt. Hochstaufen, SE Germany	Variable	1–4	3.3 $\pm$ 0.8 <sup>a</sup>	<i>Hainzl et al.</i> [2006]

<sup>a</sup> $c$  estimated by the authors.

**Table A7.** Estimation of  $c$  From Time Lag Between Groundwater Recharge Due to Snowmelt and Seismicity<sup>a</sup>

Location	Time Lag, Distance,		$c$ , m <sup>2</sup> /s	Reference
	Day	km		
Mt. Hood, Oregon	151 ± 7	4.5 ± 2	0.30 ± 0.22	<i>Saar and Manga</i> [2003]
Mt. St. Helens	30	3	3.4	<i>Christiansen et al.</i> [2005]
Long Valley Eastern South Moat	150	8	1	<i>Christiansen et al.</i> [2005]
Long Valley, Mammoth Mountain	30	6	13.5 3.5 <sup>b</sup>	<i>Christiansen et al.</i> [2005]
Hegben Lake, Yellowstone	30	2	1.5	<i>Christiansen et al.</i> [2005]
Yellowstone Lake, Yellowstone	30	5	9.3	<i>Christiansen et al.</i> [2005]

<sup>a</sup>Estimated values of  $c$  are as given by the author.

<sup>b</sup>Calculated using equation (5).

resulting in the non-Darcian flow [Kohl et al., 1997] consistent with our concept of  $k_s$ .

## 7. Conclusions

[72] Fluids play an important role in the triggering of seismicity. To study the poroelastic response to reservoir impoundment, lake level fluctuations, high-pressure fluid injections in boreholes, and seismicity related to geothermal operations and volcanic activity, we made the tacit assumption that we are dealing with fluid-filled fractures and with not a uniform half-space. We further assumed that the fracture permeability is much larger than that of the host rocks, so that all fluid pressures are confined to the fractures. We considered all saturated fractures to be critically stressed, so that small changes in fluid pressures can trigger seismicity.

[73] Although the permeability of rocks varies over several orders of magnitude, the results of our studies show that the permeability of fractures, where fluid pressure flow triggers seismicity, lies in a narrow range over 2 orders of magnitude, from  $5 \times 10^{-16}$  to  $5 \times 10^{-14}$  m<sup>2</sup>. We have named this range of permeability seismogenic permeability,  $k_s$  [Talwani and Chen, 1998]. Increases in fluid pressures lead to shear failure in accordance with the Coulomb failure criterion and trigger seismicity only in fractures with seismogenic permeability. That is,  $k_s$  is an intrinsic property of fractures where pore pressure diffusion leads to seismicity. Besides locations of induced seismicity, fluid flow also triggers aftershocks of large earthquakes [Nur and Booker, 1972]. Our results thus provide a constraint on the permeability of those faults. They also have direct implication on the assessment of permeabilities by a study of microseis-

**Table A8.** Calculation of  $c$  From Other Directly Measured Hydraulic Parameters

Location	Directly Measured		Reference
	Parameters	$c$ , m <sup>2</sup> /s	
Denver Fluid Injection, USA	$T, S$	1.1	<i>Hsieh and Bredehoft</i> [1981]
Calhio Waste Disposal, USA	$T, S$	0.2	<i>Wesson and Nicholson</i> [1986], <i>Nicholson et al.</i> [1988]

**Table A9.** Direct Measurement of  $k$  at Locations of Induced Seismicity

Location	Directly Measured		Reference
	Parameters	$k \times 10^{-15}$ m <sup>2</sup>	
Monticello RIS, USA	$k$	1.0	<i>Zoback and Hickman</i> [1982]
Lacq Oil Field, France	$k$	5.0	<i>Grasso</i> [1992]
Renqiu Oil Field, China	$k$	40	<i>Zhao et al.</i> [1995]
Nojima Fluid Injection, Japan	$k$	100	<i>Kitagawa et al.</i> [1999]
KTB Fluid Injection, Germany	$k$	0.005–0.3	<i>Huenges et al.</i> [1997]
Soultz Fluid Injection, France	$k$	0.3	<i>Evans et al.</i> [2005]

micity in locations of secondary recovery of hydrocarbons and geothermal exploitation (hot dry rock projects). They show that the seismicity outlines regions of seismogenic permeability and not those of the larger fractures where fluid flow occurs aseismically.

## Appendix A

[74] Tables A1–A9.

[75] **Acknowledgments.** This paper benefited from thoughtful reviews by John Townend (AE), Dave Hill, Jim Knapp, Ian Bastow, Francois Cornet, and an anonymous reviewer. K. G. thanks the Director of NGRI and Ravi Kumar for their support and the Department of Science and Technology, Government of India for a fellowship to study at the University of South Carolina.

## References

- Ali, M. I. (1989), Induced seismicity in the Tarbela Reservoir region, Pakistan, M.S. thesis, 86 pp., New Mexico State Univ., La Cruces.
- Anderson, D. L., and J. H. Whitcomb (1973), The dilatancy-diffusion model of earthquake predication, in Proceedings of the Conference on Tectonic Problems of the San Andreas Fault System, edited by R. L. Kovach and A. Nur, pp. 417–426, Stanford Univ. Press, Stanford, Calif.
- Anglin, F. M., and G. G. R. Buchbinder (1985), Induced seismicity at the LG3 Reservoir, James Bay, Quebec, Canada, *Bull. Seismol. Soc. Am.*, 75, 1067–1076.
- Audigane, P., J. Royer, and H. Kaieda (2000), Permeability characterization of the HDR Soultz and Ogachi large-scale reservoir using induced microseismicity, *Geophysics*, 67, 204–211.
- Barton, C. A., M. D. Zoback, and D. Moos (1995), Fluid flow along potentially active faults in crystalline rock, *Geology*, 23, 683–686.
- Bodvarsson, G. (1970), Confined fluids as strain meters, *J. Geophys. Res.*, 75, 2711–2718.
- Bosl, W. J., and A. Nur (2002), Aftershocks and pore fluid diffusion following the 1992 Landers earthquake, *J. Geophys. Res.*, 107(B12), 2366, doi:10.1029/2001JB000155.
- Brace, W. F. (1980), Permeability of crystalline and argillaceous rocks, *Int. J. Rock Mech. Min. Sci. Geomech. Abstr.*, 17, 241–251.
- Carder, D. S. (1945), Seismic investigations in the Boulder dam area, 1940–44 and the influence of reservoir loading on local earthquake activity, *Bull. Seismol. Soc. Am.*, 35, 175–192.
- Chen, L., and P. Talwani (2001), Mechanism of Initial Seismicity following Impoundment of the Monticello Reservoir, South Carolina, *Bull. Seismol. Soc. Am.*, 91, 1582–1594.
- Christiansen, L. B., S. Hurwitz, M. O. Saar, S. E. Ingebritsen, and P. A. Hsieh (2005), Seasonal seismicity at western United States volcanic centers, *Earth Planet. Sci. Lett.*, 240, 307–321.
- Clauser, C. (1992), Permeability of crystalline rocks, *Eos. Trans. AGU*, 73, 233–238.
- Cornet, F. H. (2000), Comment on “Large-scale in situ permeability tensors from induced microseismicity” by S. A. Shapiro, P. Audigane and J.-J. Royer, *Geophys. J. Int.*, 140, 465–469.
- Cornet, F. H., and R. H. Morin (1997), Evaluation of hydromechanical coupling in a Granite rock mass from a high-volume high-pressure

- injection experiment: Le Mayet de Montagne, France, *Int. J. Mech. Min. Sci. Geomech. Abstr.*, 34, 427.
- Cornet, F. H., and J. Yin (1995), Analysis of induced seismicity for stress field determination and pore pressure mapping, *Pure Appl. Geophys.*, 145, 677–700.
- Cornet, F. H., J. Helm, H. Poitrenaud, and A. Etchecopar (1997), Seismic and aseismic slip induced by large fluid injections, *Pure Appl. Geophys.*, 150, 563–583.
- Cox, R.T. (1991), Possible triggering of earthquakes by underground waste disposal in the El Dorado, Arkansas area, *Seismol. Res. Lett.*, 62, 113–122.
- Davis, S., and W. D. Pennington (1989), Induced seismic deformation in the Cogdell oil field of West Texas, *Bull. Seismol. Soc. Am.*, 79, 1477–1494.
- Ding, Y. (1987), *Reservoir-Induced Seismicity* (in Chinese), 187 pp., Seismological Press, Beijing.
- Evans, K. F., A. Genter, and J. Sausse (2005), Permeability creation and damage due to massive fluid injections into granite at 3.5 km at Soultz: 1. Borehole observations, *J. Geophys. Res.*, B04203, doi:10.1029/2004JB003168.
- Ferreira, J. M., R. T. De Oliveira, M. Assumpção, J. A. M. Moreira, R. G. Pearce, and M. K. Takeya (1995), Correlation of seismicity and water level in the Acu Reservoir—An example from Northeast Brazil, *Bull. Seismol. Soc. Am.*, 85, 1483–1489.
- Fisher, A. T. (1998), Permeability within basaltic oceanic crust, *Rev. Geophys.*, 36, 143–182.
- Fletcher, J. B., and L. R. Sykes (1977), Earthquakes related to hydraulic mining and natural seismic activity in Western New York State, *J. Geophys. Res.*, 82, 3767–3780.
- Gough, D. I., and W. I. Gough (1970), Load-induced earthquakes at Lake Kariba: II, *Geophys. J. R. Astron. Soc.*, 21, 79–101.
- Grasso, J. R. (1992), Mechanics of seismic instabilities induced by the recovery of hydrocarbons, *Pure Appl. Geophys.*, 139, 507–534.
- Grasso, J. R., F. Guyoton, J. Fréchet, and J. F. Gamond (1992), Triggered earthquakes as stress gauges: Implication for risk re-assessment in the Grenoble area, France, *Pure Appl. Geophys.*, 139, 579–605.
- Guang, Y. (1995), Seismicity induced by cascade reservoirs in Dahau, Yantan Hydroelectric Power Station, in *Proceedings of the International Symposium on Reservoir-Induced Seismicity*, Beijing, 157–163.
- Gupta, H. K. (1983), Induced seismicity hazard mitigation through water level manipulation: A suggestion, *Bull. Seismol. Soc. Am.*, 73, 679–682.
- Gupta, H. K., and B. K. Rastogi (1976), *Dams and Earthquakes*, 229 pp., Elsevier, New York.
- Hainzl, S., T. Kraft, J. Wasserman, H. Ingel, and E. Schmedes (2006), Evidence for rainfall triggered earthquake activity, *Geophys. Res. Lett.*, 33, L19303, doi:10.1029/2006GL027642.
- Healy, J. H., W. W. Rubey, D. T. Griggs, and C. B. Raleigh (1968), The Denver earthquakes, *Science*, 161, 1301–1310.
- Hsieh, P. A., and J. D. Bredehoft (1981), A reservoir analysis of the Denver earthquakes: A case of induced seismicity, *J. Geophys. Res.*, 86, 903–920.
- Hu, Y., X. Chen, Z. Zhang, W. Ma, Z. Liu, and J. Lie (1986), Induced seismicity at Hunanzhen Reservoir, Zhejiang Province, *Seismol. Geol.*, 8, 1–26.
- Hu, P., X. Chen, and Y. Hu (1995), Induced Seismicity in Dongjiang Reservoir, In *Proceedings of the International Symposium on Reservoir-Induced Seismicity*, Beijing, 142–150.
- Huang, D., and F. Kong (1984), Discussion on the induced earthquakes in Zhelin Reservoir (in Chinese), in *Induced Seismicity in China*, pp. 124–128, Seismological Press, Beijing.
- Huenges, E., B. Engester, J. Erzinger, W. Kessels, J. Kück, and G. Pusch (1997), The permeable crust: Geohydraulic properties down to 9101 m depth, *J. Geophys. Res.*, 102, 18,255–18,266.
- Ito, T., and M. D. Zoback (2000), Fracture permeability and in-situ stress to 7 km depth in the KTB Scientific Drillhole, *Geophys. Res. Lett.*, 27(7), 1045–1048.
- Jaeger, J. C., and N. G. Cook (1969), *Fundamentals of Rock Mechanics*, 515 pp., CRC, Boca Raton, Fla.
- Kessels, K., and J. Kück (1995), Hydraulic communication in crystalline rocks between the two boreholes of the continental deep drilling programme in Germany, *Int. J. Rock Mech. Sci. Geomech. Abstr.*, 32, 37–47.
- Kitagawa, Y., N. Koizumi, K. Notsu, and G. Igarashi (1999), Water injection experiments and discharge change at the Nojima Fault in Awaji Island, Japan, *Geophys. Res. Lett.*, 26, 3173–3176.
- Klaipongpan, S., and P. Chittrakarn (1995), RIS and the monitoring network at Rajjaprabha Dam, In *Proceedings of the International Symposium on Reservoir Induced Seismicity*, Beijing, 134–141.
- Kohl, T., K. F. Evans, R. J. Hopkirk, R. Jung, and L. Rybach (1997), Observation and simulation of non-Darcian flow transients in fractured rock, *Water Resour. Res.*, 33, 407–418.
- Kraft, T., J. Wasserman, E. Schmedes, and H. Ingel (2005), Meteorological triggering of earthquake swarms at Mt. Hochstaufen, SE-Germany, *Tectonophysics*, 424, 245–258.
- Leblanc, G., and F. Anglin (1978), Induced seismicity at the Manic3 Reservoir, Quebec, *Bull. Seismol. Soc. Am.*, 68, 1469–1485.
- Lester, F. M., C. G. Bufe, K. M. Lahr, and S. W. Stewart (1975), Aftershocks of the Oroville earthquake of August 1, 1975, in *Calif. Div. of Mines and Geol., Special Rep. 124*, edited by R. W. Sherburne and C. J. Hauge, 131–138.
- Lillie, R. (1999), *Whole Earth Geophysics*, 321 pp., Prentice-Hall, Upper Saddle River, N. J.
- Mahasandana, T., and J. Pinrodé (1995), Investigation of induced seismicity at Khao Laem Reservoir, in *Proceedings of the International Symposium on Reservoir Induced Seismicity*, Beijing, 179–186.
- Murakami, H., T. Hashimoto, N. Oshiman, S. Yamaguchi, Y. Honkura, and N. Sumitomo (2001), Electrokinetic phenomena associated with water injection experiment at the Nojima fault on Awaji Island, Japan, *Isl. Arc*, 10, 244–251.
- Nicholson, C., E. Roeloffs, and R. L. Wesson (1988), The northeastern Ohio earthquake of 31 January 1986: Was it induced?, *Bull. Seismol. Soc. Am.*, 78, 188–217.
- Nur, A., and J. R. Booker (1972), Aftershocks caused by pore fluid flow?, *Science*, 175, 885–887.
- Ogasawara, H., et al. (2002), Microseismicity induced by heavy rainfall around flooded vertical ore veins, *Pure Appl. Geophys.*, 159, 91–109.
- Ohtake, M. (1974), Seismic activity induced by water injection at Matsushiro, Japan, *J. Phys. Earth*, 22, 163–174.
- Pavlin, G. B., and C. A. Langston (1983), An integrated study of reservoir-induced seismicity and Landsat. Imagery of Lake Kariba, Africa, *Photogramm. Eng. Remote Sens.*, 49, 513–525.
- Pine, R. J., and A. S. Batchelor (1984), Downward migration of shearing in jointed rock during hydraulic injections, *Int. J. Rock Mech. Min. Sci. Geomech. Abstr.*, 21, 249–263.
- Prioul, R., F. H. Cornet, C. Dorbath, L. Dorbath, M. Ogena, and E. Ramos (2000), An induced seismicity experiment across a creeping segment of the Philippine Fault, *J. Geophys. Res.*, 105(B6), 13,595–13,612.
- Raleigh, C. B., J. H. Healy, and J. D. Bredehoft (1976), An experiment in earthquake control at Rangely, Colorado, *Science*, 191, 1230–1237.
- Rastogi, B. K., R. K. Chadha, and I. P. Raju (1986a), Seismicity near Bhasta Reservoir, Maharashtra, India, *Phys. Earth Planet. Inter.*, 44, 134–141.
- Rastogi, B. K., B. R. Rao, and C. V. R. K. Rao (1986b), Microearthquake investigations near Sriramsagar, Andhra Pradesh State, India, *Pure Appl. Geophys.*, 44, 179–199.
- Rastogi, B. K., R. K. Chadha, C. S. P. Sarma, P. Mandal, H. V. S. Satyanarayana, I. P. Raju, N. Kumar, C. Satyamurthy, and A. N. Rao (1997a), Seismicity at Warna Reservoir (near Koyna) through 1995, *Bull. Seismol. Soc. Am.*, 87, 1484–1494.
- Rastogi, B. K., P. Mandal, and N. Kumar (1997b), Seismicity around Dhamni Dam, Maharashtra, India, *Pure Appl. Geophys.*, 150, 493–509.
- Roeloffs, E. A. (1988), Fault stability changes induced beneath a reservoir with cyclic variations in water level, *J. Geophys. Res.*, 83, 2107–2124.
- Roeloffs, E. (1996), Poroelastic techniques in the study of earthquake-related hydrologic phenomena, *Adv. Geophys.*, 37, 136–195.
- Rojstaczer, S. A., S. Wolf, and R. Michel (1995), Permeability enhancement in the shallow crust as a cause of earthquake-induced hydrological changes, *Nature*, 373, 237–239.
- Roth, P., N. Pavoni, and N. Deichmann (1992), Seismotectonics of the eastern Swiss Alps and evidence for precipitation-induced variations of seismic activity, *Tectonophysics*, 207, 183–197.
- Saar, M. O., and M. Manga (2003), Seismicity induced by seasonal groundwater recharge at Mt. Hood, Oregon, *Earth Planet. Sci. Lett.*, 214, 605–618.
- Sasaki, S. (1998), Characteristics of microseismic events induced during hydraulic fracturing experiments at the Hijiori hot dry rock geothermal energy site, Yamagata, Japan, *Tectonophysics*, 289, 171–188.
- Saxena, S. K., G. A. Metin, and A. Sengupta (1988), Reservoir induced seismicity: A new model, *Int. J. Numer. Anal. Methods Geomech.*, 12, 263–281.
- Scholz, C. H., L. R. Sykes, and Y. P. Aggarwal (1973), Earthquake prediction: A physical basis, *Science*, 181, 803–810.
- Scotti, O., and F. H. Cornet (1994), In-situ evidence for fluid-induced aseismic slip events along fault zones, *Int. J. Rock Mech. Min. Sci. Geomech. Abstr.*, 31, 347–358.
- Shapiro, S. A., E. Huenges, and G. Borm (1997), Estimating the crust permeability from fluid-injection-induced seismic emission at the KTB site, *Geophys. J. Int.*, 131, F15–F18.
- Shapiro, S. A., R. Patzig, E. Rothert, and J. Rindschwentner (2003), Triggering of Seismicity by Pore-pressure Perturbations: Permeability-related Signatures of the Phenomenon, *Pure Appl. Geophys.*, 160, 1051–1066.

- Sharp, J. C., and Y. N. T. Maini (1972), Fundamental considerations on the hydraulic characteristics of joints in rock. Percolation Through Fissured Rock T1-F1-15, edited by Wittke, W., International Society of Rock Mechanics, Stuttgart.
- Sibson, R. F. (2001), Seismogenic framework for hydrothermal transport and ore deposition, *Rev. Econ. Geol.*, *14*, 25–50.
- Simpson, D. W., and S. K. Negmatullaev (1981), Induced seismicity at Nurek Reservoir, *Bull. Seismol. Soc. Am.*, *71*, 1561–1586.
- Skempton, A. W. (1954), The pore pressure coefficients A and B, *Geotechnique*, *4*, 143–147.
- Soboleva, O. V., and U. A. Mamadaliev (1976), The influence of the Nurek Reservoir on local earthquake activity, *Eng. Geol.*, *10*, 239–253.
- Tadokoro, K., M. Ando, and K. Nishigami (2000), Induced earthquakes accompanying the water injection experiment at the Nojima fault zone, Japan: seismicity and its migration, *J. Geophys. Res.*, *105*, 6089–6104.
- Talwani, P. (1976), Earthquakes associated with the Clark Hill Reservoir, South Carolina—A case of induced seismicity, *Eng. Geol.*, *10*, 239–253.
- Talwani, P. (1981), Hydraulic diffusivity and reservoir induced seismicity, 48 pp., Final Tech. Rep., U.S. Geol. Surv., Reston, Va.
- Talwani, P. (1997), On the nature of reservoir-induced seismicity, *Pure Appl. Geophys.*, *150*, 473–492.
- Talwani, P., and S. Acree (1984), Pore pressure diffusion and the mechanism of reservoir induced seismicity, *Pure Appl. Geophys.*, *122*, 947–965.
- Talwani, P., and S. Acree (1987), *Induced seismicity at Monticello Reservoir: A case study*, 271 pp., Final Tech. Rep., U.S. Geol. Surv., Reston, Va.
- Talwani, P., and L. Chen (1998), Are seismogenic faults associated with a characteristic permeability? Introducing, “Seismogenic” permeability,  $k_s$ , *Eos. Trans. AGU*, *79*(45), Fall Meeting Suppl. F583.
- Talwani, P., J. S. Cobb, and M. F. Schaeffer (1999), In situ measurement of hydraulic properties of a shear zone in northwestern South Carolina, *J. Geophys. Res.*, *104*, 14,993–15,003.
- Tezuka, K., and H. Niitsuma (2000), Stress estimated using microseismic clusters and its relationship to the fracture system of the Hijiori hot dry rock reservoir, *Eng. Geol.*, *56*, 47–62.
- Topozada, T. R., and C. H. Cramer (1978), Ukiah earthquake, 25 March 1978, seismicity possibly induced by Lake Mendocino, California, *Geology*, *31*, 2775–2781.
- Townend, J., and M. D. Zoback (2000), How faulting keeps the crust strong, *Geology*, *28*, 399–402.
- Ventura, G., and G. Vilardo (1999), Seismic-based estimate of hydraulic parameters at Vesuvius Volcano, *Geophys. Res. Lett.*, *26*, 887–890.
- Wang, H. F. (2000), *Theory of Linear Poroelasticity*, 287 pp., Princeton Univ. Press, Princeton N. J.
- Wang, M., M. Yang, Y. Hu, T. Li, Y. Chin, Y. Chen, and J. Feng (1976), Mechanism of the reservoir impounding earthquakes at Hisfengkiang and a preliminary endeavor to discuss their cause, *Eng. Geol.*, *10*, 331–359.
- Weast, R. C. (1987), *CRC Handbook of chemistry and physics*, CRC Press, Inc., Boca Raton, F-37.
- Wesson, R. L., and C. Nicholson (1986), *Studies of the January 31, 1986 Northern Ohio earthquake*, 130 pp., U.S. Geol. Surv., VA.
- Whitcomb, J. H., J. D. Garmany, and D. L. Anderson (1973), Earthquake prediction: Variation of seismic velocities before the San Francisco earthquake, *Science*, *180*, 632–635.
- Wolf, L. W., C. A. Rowe, and R. B. Horner (1997), Periodic Seismicity near Mt. Ogden on the Alaska-British Columbia border: A case for hydrologically triggered earthquakes?, *Bull. Seismol. Soc. Am.*, *87*, 1473–1483.
- Zhao, G., H. Chen, S. Ma, and D. Zhang (1995), Research on earthquakes induced by water injection in China, *Pure Appl. Geophys.*, *145*, 59–68.
- Zoback, M., and H.-P. Harjes (1997), Injection-induced earthquakes and crustal stress at 9 km depth at the KTB deep drilling site, Germany, *J. Geophys. Res.*, *102*, 18477–18491.
- Zoback, M. D., and S. Hickman (1997), In situ study of the physical mechanisms controlling induced seismicity at Monticello Reservoir, South Carolina, *J. Geophys. Res.*, *87*, 6959–6974.
- Zhong, Y., X. Jiang, K. Pan, and L. Xiao (1995), Study of the generating condition of earthquakes at Shenwo Reservoir, Liaoning Province, In *Proceedings of the International Symposium on Reservoir-Induced Seismicity*, Beijing, 171–178.

L. Chen and P. Talwani, Department of Geol. Sciences, Univ. of South Carolina, Columbia, SC, USA. (talwani@geol.sc.edu)

K. Gahalaut, National Geophysical Research Institute, Hyderabad, India.